Available online at www.sciencedirect.com
SCIENCE DIRECT®
Journal of Computational Physics 197 (2004) 58–85
JOURNAL OF COMPUTATIONAL PHYSICS
www.elsevier.com/locate/jcp

Standardized pseudospectral formulation of the inviscid supersonic blunt body problem ☆

Gregory P. Brooks [a,1], Joseph M. Powers [b,*,2]

[a] Air Force Research Laboratory, Wright-Patterson AFB, OH 45433, USA
[b] Department of Aerospace and Mechanical Engineering, University of Notre Dame, 372 Fitzpatrick Hall of Engineering, Notre Dame, IN 46556-5637, USA

Received 21 February 2003; received in revised form 24 November 2003; accepted 25 November 2003
Available online 23 December 2003

Abstract

A highly accurate pseudospectral numerical approximation to the generalized coordinate, nonconservative form of the Euler equations is implemented for supersonic flow over an axisymmetric blunt body geometry; shock fitting is employed to maintain global accuracy and minimize the corrupting influence of numerical viscosity. The variables in the Euler equations as well as the physical grid coordinates are collocated via Lagrange interpolating polynomials and the problem is then cast in the standard form of a large system of ordinary differential equations, $d\mathbf{x}/d\tau = \mathbf{q}(\mathbf{x})$, which can be solved using standard solution techniques that do not require an explicit criteria for the minimum time step. Code verification is performed by demonstrating through a series of grid refinement tests that the error in the approximation to a Taylor–Maccoll solution converges to 10^{-12}. Grid refinement tests for flow over a blunt body show convergence of the numerical error also to 10^{-12}. The code is validated for supersonic flow over a blunt body by comparison with the modified Newtonian approximation for the surface pressure distribution and empirical predictions for the shock shape. The ability of the method to capture unsteady flow phenomena is demonstrated on the problem of a planar acoustic wave interacting with an attached shock.

Keywords: Shock fitting; Supersonic blunt body; Euler equations; Pseudospectral method; System of ordinary differential equations

☆ This study has received primary support from the United States Air Force Palace Knight Program and additional support from Los Alamos National Laboratory.
* Corresponding author. Tel.: +574-631-5978; fax: +574-631-8341.
E-mail addresses: Gregory.Brooks@wpafb.af.mil (G.P. Brooks), powers@nd.edu (J.M. Powers).
[1] Research Aerospace Engineer.
[2] Associate Professor.

0021-9991/$ - see front matter
doi:10.1016/j.jcp.2003.11.017

1. Introduction

As a prerequisite for developing a new technique for shape optimization of bodies in supersonic flow [1], we require a highly accurate flow solution technique. Consequently, in this work, we present a pseudospectral numerical approximation to the solution for the supersonic, inviscid flow of a calorically perfect ideal gas over an axisymmetric blunt body in standardized form. The shock is fitted since approximation of discontinuous solutions with high order polynomials exhibits the Gibbs phenomenon in the form of global oscillations in the solution [2]. These oscillations can cause the numerical scheme to become unstable, and attempts to remove the oscillations by spectral filtering or by addition of artificial viscosity significantly reduces the accuracy of the numerical method. The more common alternative of shock capturing, while generally stable and nonoscillatory, yields only first order accuracy [3].

While the main motivation of our work is to have high accuracy steady state solutions available for use in a shape optimization procedure, we note there are outstanding questions regarding numerical and physical instabilities in multi-dimensional shock dynamics for which a standard formulation of $d\mathbf{x}/d\tau = \mathbf{q}(\mathbf{x})$ has value. As stated in [4–11], the issues of shock stability are controversial since it is not clear what effects are real and which ones are purely numerical artifacts. Although shock stability will not be investigated in the current work, the shock fitting method used here is the most appropriate for addressing fundamental stability questions for inviscid flows due to the significantly low level of numerical viscosity inherent in the method. Furthermore, should a physical instability exist, one would like to have a numerical method with sufficient robustness to automatically select the time step so as to resolve the dynamics, and because of the additional dynamic equations which arise from the unsteady shock wave, a simple CFL criterion is insufficient in the general case. Fortunately, the casting of the discretized governing equations into the form $d\mathbf{x}/d\tau = \mathbf{q}(\mathbf{x})$ allows the use of standard software packages which have automatic time step selection, precluding the necessity of an explicit condition for numerical stability. As such, we place emphasis here on obtaining this standard form.

We briefly review the literature on solutions to the supersonic flow over blunt body geometries. Rusanov [12] and Hayes and Probstein [13] have given thorough reviews of early contributions, of which a few will be mentioned. Two methodologies for calculating solutions to the supersonic flow about a blunt body are the direct and inverse methods. In the direct method the body shape is specified, and then the shock shape and flow field are calculated. In the inverse method the shock shape is specified, and the body shape which would support that shock shape is calculated. At first, studies concerning the inverse problem were based on series expansion of the governing equations in the vicinity of the shock wave [14]. Later, numerical solutions to the inverse, supersonic blunt body problem were performed by Garabedian and Lieberstein [15] and Van Dyke [16]. Evans and Harlow [17] were the first to generate numerical solutions to the direct problem by integrating the unsteady Euler equations to a relaxed steady state solution. Moretti and Abbett [18] used finite differences and fitting of the shock to generate accurate solutions of the Euler equations about a blunt body; this laid the foundation for subsequent shock fitting numerical schemes. Pseudospectral approximations to the Euler equations employing shock fitting with spectral filtering were first performed by Hussaini et al. [19] and without spectral filtering by Kopriva [20]. The numerical technique employed in the current paper builds on the work by Kopriva [20,21], and Brooks and Powers [22].

We briefly review the pseudospectral methods. An early unified mathematical description of the theory of spectral and pseudospectral methods was given by Gottlieb and Orszag [2]. Significant advances occurred in the late 1970s and early 1980s and are well documented by Canuto et al. [23], with particular application to fluid dynamics. For a more recent review, see [24].

There does not appear to be complete consensus in the literature for the definition of pseudospectral; a definition is adopted here which we believe useful and consistent with that of Fornberg [25]. We define a pseudospectral method to be a collocation type of method of weighted residuals, as defined by Finlayson

[26], in which the error in the solution to the governing equations is driven to zero at collocation points; the flow quantities are represented in terms of global Lagrange interpolating polynomials defined at the collocation points. The spatial derivatives of the flow quantities are then calculated by differentiating the Lagrange interpolating polynomials. Efficient algorithms for calculating derivatives of Lagrange interpolating polynomials on arbitrary grids can be found in [25]; these algorithms were used in the current work. A property of the pseudospectral method is that approximations to derivatives have global support, making it equivalent to a finite difference scheme with a stencil that extends over the entire domain. As the number of points is increased, the size of the stencil grows, leading to a higher order accurate solution.

2. Supersonic blunt body flow and pseudospectral solver

2.1. Standard formulation

Before presenting the geometry, governing equations, boundary and initial conditions for the blunt body problem, we will briefly outline the procedure for formulating this problem as a system of ordinary differential equations (ODEs). The Euler equations, physical grid evolution equations, shock velocity equation, and boundary conditions defined over the computational domain

$$\Omega : \{\xi \in [0,1], \eta \in [0,1]\}, \tag{1}$$

and bounded by S, can be written in the form of the following coupled system of time-dependent partial differential and algebraic equations

$$\frac{\partial \mathbf{y}}{\partial \tau} + \mathbf{f}\left(\mathbf{y}, \frac{\partial \mathbf{y}}{\partial \xi}, \frac{\partial \mathbf{y}}{\partial \eta}\right) = \mathbf{0}, \tag{2}$$

$$\mathbf{g}\left(\mathbf{y}, \frac{\partial \mathbf{y}}{\partial \xi}, \frac{\partial \mathbf{y}}{\partial \eta}\right) = \mathbf{0}, \tag{3}$$

along with the initial conditions

$$\mathbf{y}(\xi, \eta, 0) = \mathbf{y}_0(\xi, \eta), \tag{4}$$

where ξ and η are independent spatial variables in the computational space, and $\mathbf{f}$ and $\mathbf{g}$ are nonlinear functions of the dependent variables $\mathbf{y}(\xi, \eta, \tau)$ and its spatial derivatives. All of the algebraic constraints, Eq. (3), are boundary conditions and thus apply only on S.

Approximating $\mathbf{y}(\xi, \eta, \tau)$ and its spatial derivatives via global Lagrange interpolating polynomials, the system of partial differential and algebraic equations in Eqs. (2) and (3) reduce to the following system of P_2 differential algebraic equations:

$$\frac{\mathrm{d}y_p(\tau)}{\mathrm{d}\tau} = f_p(y_1, \ldots, y_{P_2}), \quad p = 1, \ldots, P_1, \tag{5}$$

$$0 = g_{p'}(y_1, \ldots, y_{P_2}), \quad p' = P_1 + 1, \ldots, P_2, \tag{6}$$

with initial conditions from Eq. (4)

$$y_p(0) = y_{0p}, \quad p = 1, \ldots, P_1. \tag{7}$$

Here $y_1(\tau),\ldots,y_{P_2}(\tau)$ are the flow quantities, physical grid coordinates, and shock velocity evaluated at nodal points on an $(N+1)\times(M+1)$ mesh. Solving for the $y_{p'}(\tau)$, $p'=P_1+1,\ldots,P_2$, as explicit functions of the y_p, $p=1,\ldots,P_1$, i.e.

$$y_{p'}(\tau)=\widehat{g}_{p'}(y_1,\ldots,y_{P_1}),\quad p'=P_1+1,\ldots,P_2. \tag{8}$$

Eqs. (5) and (6) are converted into the following system of P_1 ODEs:

$$\frac{\mathrm{d}x_p(\tau)}{\mathrm{d}\tau}=q_p(x_1,\ldots,x_{P_1}),\quad p=1,\ldots,P_1, \tag{9}$$

where

$$q_p(x_1,\ldots,x_{P_1})\equiv f_p\Big(y_1,\ldots,y_{P_1},\widehat{g}_{p'}(y_1,\ldots,y_{P_1})\Big),\quad p=1,\ldots,P_1,\ \ p'=P_1+1,\ldots,P_2, \tag{10}$$

and

$$x_p(\tau)=y_p(\tau),\quad p=1,\ldots,P_1. \tag{11}$$

The accompanying initial conditions are

$$x_p(0)=x_{0p},\quad p=1,\ldots,P_1. \tag{12}$$

In compact vector notation, Eq. (9) is

$$\frac{\mathrm{d}\mathbf{x}}{\mathrm{d}\tau}=\mathbf{q}(\mathbf{x}), \tag{13}$$

with accompanying initial conditions

$$\mathbf{x}(0)=\mathbf{x}_0 \tag{14}$$

from Eq. (12).

2.2. Governing equations

The two-dimensional, axisymmetric Euler equations for a calorically perfect ideal gas are in dimensionless form:

$$\frac{\partial\rho}{\partial t}+u\frac{\partial\rho}{\partial r}+w\frac{\partial\rho}{\partial z}+\rho\left(\frac{\partial u}{\partial r}+\frac{\partial w}{\partial z}+\frac{u}{r}\right)=0, \tag{15}$$

$$\frac{\partial u}{\partial t}+u\frac{\partial u}{\partial r}+w\frac{\partial u}{\partial z}+\frac{1}{\rho}\frac{\partial p}{\partial r}=0, \tag{16}$$

$$\frac{\partial w}{\partial t}+u\frac{\partial w}{\partial r}+w\frac{\partial w}{\partial z}+\frac{1}{\rho}\frac{\partial p}{\partial z}=0, \tag{17}$$

$$\frac{\partial p}{\partial t}+u\frac{\partial p}{\partial r}+w\frac{\partial p}{\partial z}+\gamma p\left(\frac{\partial u}{\partial r}+\frac{\partial w}{\partial z}+\frac{u}{r}\right)=0, \tag{18}$$

where ρ is density, p is pressure, u and w are the velocities in the radial and axial directions, respectively, r is the radial coordinate, z is the axial coordinate, t is time, and γ is the ratio of specific heats. The dimensional form for pressure, p^*, density, ρ^*, and r^* and z^* components of velocity, u^* and w^*, respectively, are recovered by the following equations:

$$p^* = pp^*_\infty, \tag{19}$$

$$\rho^* = \rho\rho^*_\infty, \tag{20}$$

$$u^* = u\sqrt{p^*_\infty/\rho^*_\infty}, \quad w^* = w\sqrt{p^*_\infty/\rho^*_\infty}, \tag{21}$$

where dimensional quantities are denoted by a $*$, and freestream quantities are denoted by ∞. The dimensional space and time variables are

$$z^* = zL, \quad r^* = rL, \tag{22}$$

$$t^* = tL/\sqrt{p^*_\infty/\rho^*_\infty}, \tag{23}$$

where L is the length of the body. The freestream flow is at zero angle of attack so that the component of freestream velocity in the r direction, $u_\infty = 0$.

Defining the entropy to be s, we have, for a calorically perfect ideal gas with zero freestream entropy,

$$s = \ln\left(\frac{p}{\rho^\gamma}\right), \tag{24}$$

where the entropy is nondimensionalized by the the specific heat at constant volume, c^*_v,

$$s^* = sc^*_v. \tag{25}$$

To facilitate the solution to the Euler equations for time-varying geometry, Eqs. (15)–(18) are rewritten in terms of a general body-fitted coordinate system, $\xi(z,r,t)$, $\eta(z,r,t)$ and $\tau(z,r,t)$. Employing the chain rule of differentiation

$$\begin{aligned}
\frac{\partial}{\partial z} &= \frac{\partial\xi}{\partial z}\frac{\partial}{\partial\xi} + \frac{\partial\eta}{\partial z}\frac{\partial}{\partial\eta} + \frac{\partial\tau}{\partial z}\frac{\partial}{\partial\tau},\\
\frac{\partial}{\partial r} &= \frac{\partial\xi}{\partial r}\frac{\partial}{\partial\xi} + \frac{\partial\eta}{\partial r}\frac{\partial}{\partial\eta} + \frac{\partial\tau}{\partial r}\frac{\partial}{\partial\tau},\\
\frac{\partial}{\partial t} &= \frac{\partial\xi}{\partial t}\frac{\partial}{\partial\xi} + \frac{\partial\eta}{\partial t}\frac{\partial}{\partial\eta} + \frac{\partial\tau}{\partial t}\frac{\partial}{\partial\tau},
\end{aligned} \tag{26}$$

and taking $\tau(z,r,t) = t$, the nondimensional form of Eqs. (15)–(18) in generalized coordinates is

$$\frac{\partial\rho}{\partial\tau} + \widehat{u}\frac{\partial\rho}{\partial\xi} + \widehat{w}\frac{\partial\rho}{\partial\eta} + \rho\left(\frac{\partial\xi}{\partial r}\frac{\partial u}{\partial\xi} + \frac{\partial\xi}{\partial z}\frac{\partial w}{\partial\xi} + \frac{\partial\eta}{\partial r}\frac{\partial u}{\partial\eta} + \frac{\partial\eta}{\partial z}\frac{\partial w}{\partial\eta}\right) + \frac{\rho u}{r} = 0, \tag{27}$$

$$\frac{\partial u}{\partial\tau} + \widehat{u}\frac{\partial u}{\partial\xi} + \widehat{w}\frac{\partial u}{\partial\eta} + \frac{1}{\rho}\left(\frac{\partial\xi}{\partial r}\frac{\partial p}{\partial\xi} + \frac{\partial\eta}{\partial r}\frac{\partial p}{\partial\eta}\right) = 0, \tag{28}$$

$$\frac{\partial w}{\partial \tau}+\widehat{u}\frac{\partial w}{\partial \xi}+\widehat{w}\frac{\partial w}{\partial \eta}+\frac{1}{\rho}\left(\frac{\partial \xi}{\partial z}\frac{\partial p}{\partial \xi}+\frac{\partial \eta}{\partial z}\frac{\partial p}{\partial \eta}\right)=0, \tag{29}$$

$$\frac{\partial p}{\partial \tau}+\widehat{u}\frac{\partial p}{\partial \xi}+\widehat{w}\frac{\partial p}{\partial \eta}+\gamma p\left(\frac{\partial \xi}{\partial r}\frac{\partial u}{\partial \xi}+\frac{\partial \xi}{\partial z}\frac{\partial w}{\partial \xi}+\frac{\partial \eta}{\partial r}\frac{\partial u}{\partial \eta}+\frac{\partial \eta}{\partial z}\frac{\partial w}{\partial \eta}\right)+\frac{\gamma p u}{r}=0, \tag{30}$$

where the contravariant velocity components $\widehat{u}$ and $\widehat{w}$ are

$$\widehat{u}=\frac{\partial \xi}{\partial t}+u\frac{\partial \xi}{\partial r}+w\frac{\partial \xi}{\partial z}, \tag{31}$$

$$\widehat{w}=\frac{\partial \eta}{\partial t}+u\frac{\partial \eta}{\partial r}+w\frac{\partial \eta}{\partial z}. \tag{32}$$

The following standard relations between the metrics and inverse metrics will be necessary

$$\begin{aligned}
&\frac{\partial \xi}{\partial z}=\frac{1}{J}\frac{\partial r}{\partial \eta}, \quad \frac{\partial \eta}{\partial z}=-\frac{1}{J}\frac{\partial r}{\partial \xi},\\
&\frac{\partial \xi}{\partial r}=-\frac{1}{J}\frac{\partial z}{\partial \eta}, \quad \frac{\partial \eta}{\partial r}=\frac{1}{J}\frac{\partial z}{\partial \xi},\\
&\frac{\partial \xi}{\partial t}=\frac{\left(\frac{\partial r}{\partial \tau}\frac{\partial z}{\partial \eta}-\frac{\partial r}{\partial \eta}\frac{\partial z}{\partial \tau}\right)}{J}, \quad \frac{\partial \eta}{\partial t}=\frac{\left(\frac{\partial r}{\partial \xi}\frac{\partial z}{\partial \tau}-\frac{\partial r}{\partial \tau}\frac{\partial z}{\partial \xi}\right)}{J},\\
&J=\frac{\partial r}{\partial \eta}\frac{\partial z}{\partial \xi}-\frac{\partial r}{\partial \xi}\frac{\partial z}{\partial \eta},
\end{aligned} \tag{33}$$

where J is the determinant of the metric Jacobian matrix.

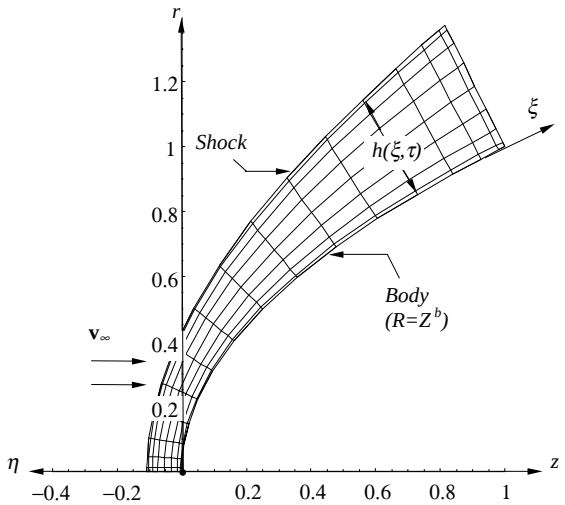

Fig. 1. Schematic of shock-fitted high Mach number flow over an axisymmetric blunt body including computational (ξ,η) and physical (r,z) coordinates.

2.3. Computational and physical coordinates

The physical domain of the blunt body problem, Fig. 1, is mapped to the computational domain, $\xi \in [0,1]$, $\eta \in [0,1]$, in such a way that the body surface lies along the computational boundary $(\xi,0)$, the shock lies along the boundary $(\xi,1)$, the symmetry axis is a third boundary at $(0,\eta)$, and the fourth boundary at $(1,\eta)$ is a supersonic outflow. The transformation between the physical coordinates (r,z) and computational coordinates (ξ,η) is taken to be

$$r(\xi,\eta,\tau) = R(\xi) + \frac{\eta \frac{\mathrm{d}Z(\xi)}{\mathrm{d}\xi} h(\xi,\tau)}{\sqrt{\left(\frac{\mathrm{d}R(\xi)}{\mathrm{d}\xi}\right)^2 + \left(\frac{\mathrm{d}Z(\xi)}{\mathrm{d}\xi}\right)^2}}, \tag{34}$$

$$z(\xi,\eta,\tau) = Z(\xi) - \frac{\eta \frac{\mathrm{d}R(\xi)}{\mathrm{d}\xi} h(\xi,\tau)}{\sqrt{\left(\frac{\mathrm{d}R(\xi)}{\mathrm{d}\xi}\right)^2 + \left(\frac{\mathrm{d}Z(\xi)}{\mathrm{d}\xi}\right)^2}}, \tag{35}$$

where the nonlinear function $h(\xi,\tau)$ must be specified to completely determine the mapping, and $R(\xi)$ and $Z(\xi)$ are known functions. After manipulation, the transformations in Eqs. (34) and (35) yield the following identity:

$$h(\xi,\tau) = \sqrt{(z(\xi,1,\tau) - z(\xi,0,\tau))^2 + (r(\xi,1,\tau) - r(\xi,0,\tau))^2}, \tag{36}$$

from which it is seen that the function $h(\xi,\tau)$ is the distance in r–z space between the body surface, $\eta = 0$, and the shock, $\eta = 1$, along lines of constant ξ. The function $h(\xi,\tau)$ is subsequently referred to as the shock distance function. We see that Eqs. (34) and (35) form an implicit algebraic equation for the coordinate transformation. It is apparent from Eqs. (34) and (35) that the functions $R(\xi)$ and $Z(\xi)$ parameterize the blunt body surface, $\eta = 0$, i.e.

$$\begin{aligned} r(\xi,0,\tau) &= R(\xi), \\ z(\xi,0,\tau) &= Z(\xi), \end{aligned} \tag{37}$$

and that the body surface is not a function of time. The transformations in Eqs. (34) and (35) have been constructed so that lines of constant ξ are normal to the body surface and have no curvature in r–z space.

The time evolution equations for the physical grid $r(\xi,\eta,\tau)$, and $z(\xi,\eta,\tau)$ can be found by differentiating Eqs. (34) and (35) with respect to time as follows:

$$\frac{\partial}{\partial\tau} r(\xi,\eta,\tau) = \frac{\eta \frac{\mathrm{d}Z(\xi)}{\mathrm{d}\xi} v(\xi,\tau)}{\sqrt{\left(\frac{\mathrm{d}R(\xi)}{\mathrm{d}\xi}\right)^2 + \left(\frac{\mathrm{d}Z(\xi)}{\mathrm{d}\xi}\right)^2}}, \tag{38}$$

$$\frac{\partial}{\partial\tau} z(\xi,\eta,\tau) = -\frac{\eta \frac{\mathrm{d}R(\xi)}{\mathrm{d}\xi} v(\xi,\tau)}{\sqrt{\left(\frac{\mathrm{d}R(\xi)}{\mathrm{d}\xi}\right)^2 + \left(\frac{\mathrm{d}Z(\xi)}{\mathrm{d}\xi}\right)^2}}, \tag{39}$$

where the shock velocity function $v(\xi,\tau)$ is

$$v(\xi,\tau) = \frac{\partial}{\partial\tau} h(\xi,\tau). \tag{40}$$

2.4. Boundary conditions

The kinematic boundary condition of no mass flux at the body surface requires that the velocity component normal to the body surface, $v_{\mathrm{BN}}(\xi,\tau)$, be equal to zero, i.e.

$$v_{\mathrm{BN}}(\xi,\tau) = \widehat{w}(\xi,0,\tau) = 0. \tag{41}$$

In order to formulate a numerical boundary condition at the body for ρ, u, w, and p, Eqs. (27)–(30) are written in the following form:

$$\frac{\partial \mathbf{z}}{\partial \tau} + \mathbf{A}\frac{\partial \mathbf{z}}{\partial \xi} + \mathbf{B}\frac{\partial \mathbf{z}}{\partial \eta} + \mathbf{s} = \mathbf{0}, \tag{42}$$

where

$$\mathbf{z} = \begin{bmatrix} \rho \\ u \\ w \\ p \end{bmatrix}, \quad \mathbf{s} = \begin{bmatrix} \rho u/r \\ 0 \\ 0 \\ \gamma p u/r \end{bmatrix}, \tag{43}$$

$$\mathbf{A} = \begin{bmatrix} \widehat{u} & \rho\frac{\partial\xi}{\partial r} & \rho\frac{\partial\xi}{\partial z} & 0 \\ 0 & \widehat{u} & 0 & \frac{1}{\rho}\frac{\partial\xi}{\partial r} \\ 0 & 0 & \widehat{u} & \frac{1}{\rho}\frac{\partial\xi}{\partial z} \\ 0 & \gamma p\frac{\partial\xi}{\partial r} & \gamma p\frac{\partial\xi}{\partial z} & \widehat{u} \end{bmatrix}, \quad \mathbf{B} = \begin{bmatrix} \widehat{w} & \rho\frac{\partial\eta}{\partial r} & \rho\frac{\partial\eta}{\partial z} & 0 \\ 0 & \widehat{w} & 0 & \frac{1}{\rho}\frac{\partial\eta}{\partial r} \\ 0 & 0 & \widehat{w} & \frac{1}{\rho}\frac{\partial\eta}{\partial z} \\ 0 & \gamma p\frac{\partial\eta}{\partial r} & \gamma p\frac{\partial\eta}{\partial z} & \widehat{w} \end{bmatrix}. \tag{44}$$

The flux Jacobian matrix $\mathbf{B}$ is then decomposed as

$$\mathbf{B} = \mathbf{P}^{-1}\mathbf{\Lambda}_\eta\mathbf{P}, \tag{45}$$

where the square matrix $\mathbf{P}$ contains the left eigenvectors of $\mathbf{B}$ in its rows; the diagonal matrix $\mathbf{\Lambda}_\eta$ contains the eigenvalues of $\mathbf{B}$ in its diagonal; and $\mathbf{P}^{-1}$ is the inverse of $\mathbf{P}$. Substituting Eq. (45) into Eq. (42) and premultiplying by $\mathbf{P}$ yields the following characteristic formulation [27,28] of the governing equations:

$$\mathbf{P}\frac{\partial \mathbf{z}}{\partial \tau} + \mathbf{P}\mathbf{A}\frac{\partial \mathbf{z}}{\partial \xi} + \mathbf{\Lambda}_\eta\mathbf{P}\frac{\partial \mathbf{z}}{\partial \eta} + \mathbf{P}\mathbf{s} = \mathbf{0}. \tag{46}$$

The diagonal eigenvalue matrix $\mathbf{\Lambda}_\eta$ and the left eigenvector matrix $\mathbf{P}$ are

$$\mathbf{\Lambda}_\eta = \begin{bmatrix} \widehat{w} & 0 & 0 & 0 \\ 0 & \widehat{w} & 0 & 0 \\ 0 & 0 & \widehat{w} - c\sqrt{\left(\frac{\partial\eta}{\partial z}\right)^2 + \left(\frac{\partial\eta}{\partial r}\right)^2} & 0 \\ 0 & 0 & 0 & \widehat{w} + c\sqrt{\left(\frac{\partial\eta}{\partial z}\right)^2 + \left(\frac{\partial\eta}{\partial r}\right)^2} \end{bmatrix}, \tag{47}$$

$$\mathbf{P} = \begin{bmatrix} 0 & -\frac{\frac{\partial\eta}{\partial z}\frac{\partial\eta}{\partial r}}{\left(\frac{\partial\eta}{\partial z}\right)^2+\left(\frac{\partial\eta}{\partial r}\right)^2} & \frac{\left(\frac{\partial\eta}{\partial z}\right)^2}{\left(\frac{\partial\eta}{\partial z}\right)^2+\left(\frac{\partial\eta}{\partial r}\right)^2} & 0 \\ 1 & 0 & 0 & -\frac{1}{c^2} \\ 0 & -\frac{\rho c\frac{\partial\eta}{\partial z}}{2\sqrt{\left(\frac{\partial\eta}{\partial z}\right)^2+\left(\frac{\partial\eta}{\partial r}\right)^2}} & -\frac{\rho c\frac{\partial\eta}{\partial r}}{2\sqrt{\left(\frac{\partial\eta}{\partial z}\right)^2+\left(\frac{\partial\eta}{\partial r}\right)^2}} & \frac{1}{2} \\ 0 & \frac{\rho c\frac{\partial\eta}{\partial z}}{2\sqrt{\left(\frac{\partial\eta}{\partial z}\right)^2+\left(\frac{\partial\eta}{\partial r}\right)^2}} & \frac{\rho c\frac{\partial\eta}{\partial r}}{2\sqrt{\left(\frac{\partial\eta}{\partial z}\right)^2+\left(\frac{\partial\eta}{\partial r}\right)^2}} & \frac{1}{2} \end{bmatrix}, \tag{48}$$

where $c = \sqrt{\gamma p/\rho}$ is the dimensionless acoustic speed. Since $\widehat{w}$ is everywhere negative and since $\|\widehat{w}\| < \|c\sqrt{(\partial\eta/\partial z)^2 + (\partial\eta/\partial r)^2}\|$ at $\eta = 0$, only the first three of the equations in Eq. (46) can be used in formulating numerical boundary conditions since they are associated with negative eigenvalues, $\mathbf{\Lambda}_\eta$. The fourth equation in Eq. (46) is associated with a positive eigenvalue and thus describes information propagation from inside the body which must therefore be discarded as nonphysical; in its place the physical boundary condition, Eq. (41), is employed. Making use of the fact that $\widehat{w}(\xi,0,\tau) = \frac{\partial\widehat{w}}{\partial\tau}|_{(\xi,0,\tau)} = 0$, the three differential equations from Eq. (46) to be solved at the body surface, $\eta = 0$, are cast in the following form, which is consistent with Eq. (2)

$$\left[\frac{\partial\rho}{\partial\tau} = \frac{1}{c^2}\frac{\partial p}{\partial\tau} - \widehat{u}\left(\frac{\partial\rho}{\partial\xi} - \frac{1}{c^2}\frac{\partial p}{\partial\xi}\right)\right]\Bigg|_{(\xi,0,\tau)}, \tag{49}$$

$$\frac{\partial}{\partial\tau}v_{\mathrm{BT}}(\xi,\tau) = \left.\frac{\left(\widehat{u}\left(\frac{\partial\eta}{\partial r}\frac{\partial w}{\partial\xi} - \frac{\partial\eta}{\partial z}\frac{\partial u}{\partial\xi}\right) + \frac{1}{\rho}\left(\frac{\partial\eta}{\partial r}\frac{\partial\xi}{\partial z} - \frac{\partial\eta}{\partial z}\frac{\partial\xi}{\partial r}\right)\frac{\partial p}{\partial\xi}\right)}{\sqrt{\left(\frac{\partial\eta}{\partial z}\right)^2 + \left(\frac{\partial\eta}{\partial r}\right)^2}}\right|_{(\xi,0,\tau)}, \tag{50}$$

$$\left[\frac{\partial p}{\partial\tau} = \frac{\rho c\widehat{u}\left(\frac{\partial\eta}{\partial r}\frac{\partial u}{\partial\xi} + \frac{\partial\eta}{\partial z}\frac{\partial w}{\partial\xi}\right) + c\left(\frac{\partial\eta}{\partial r}\frac{\partial\xi}{\partial r} + \frac{\partial\eta}{\partial z}\frac{\partial\xi}{\partial z}\right)\frac{\partial p}{\partial\xi}}{\sqrt{\left(\frac{\partial\eta}{\partial z}\right)^2 + \left(\frac{\partial\eta}{\partial r}\right)^2}} - \rho c^2\left(\frac{\partial\xi}{\partial r}\frac{\partial u}{\partial\xi} + \frac{\partial\xi}{\partial z}\frac{\partial w}{\partial\xi} + \frac{\partial\eta}{\partial r}\frac{\partial u}{\partial\eta} + \frac{\partial\eta}{\partial z}\frac{\partial w}{\partial\eta}\right) + c\sqrt{\left(\frac{\partial\eta}{\partial z}\right)^2 + \left(\frac{\partial\eta}{\partial r}\right)^2}\frac{\partial p}{\partial\eta} - \widehat{u}\frac{\partial p}{\partial\xi} - \frac{\rho c^2 u}{r}\right]\Bigg|_{(\xi,0,\tau)}. \tag{51}$$

The velocity components $u(\xi,0,\tau)$ and $w(\xi,0,\tau)$ are specified as following functions of v_{BT}:

$$u(\xi,0,\tau) = \left.\frac{\frac{\partial r}{\partial\xi}v_{\mathrm{BT}}(\xi,\tau)}{\sqrt{\left(\frac{\partial r}{\partial\xi}\right)^2 + \left(\frac{\partial z}{\partial\xi}\right)^2}}\right|_{(\xi,0,\tau)}, \quad w(\xi,0,\tau) = \left.\frac{\frac{\partial z}{\partial\xi}v_{\mathrm{BT}}(\xi,\tau)}{\sqrt{\left(\frac{\partial r}{\partial\xi}\right)^2 + \left(\frac{\partial z}{\partial\xi}\right)^2}}\right|_{(\xi,0,\tau)}. \tag{52}$$

At the shock boundary, the Rankine–Hugoniot relations are solved along with a compatibility equation. Specifically, the Rankine–Hugoniot relations are

$$\mathbf{v}_\infty \cdot \mathbf{e}_{\mathrm{ST}}|_{(\xi,1,\tau)} = \mathbf{v}\cdot\mathbf{e}_{\mathrm{ST}}|_{(\xi,1,\tau)}, \tag{53}$$

$$\delta_S(\xi,\tau) = \frac{\gamma-1}{\gamma+1}\delta_\infty(\xi,\tau) + \frac{2\gamma p_\infty}{(\gamma+1)\rho_\infty\delta_\infty(\xi,\tau)}, \tag{54}$$

$$p(\xi,1,\tau)=\frac{2\rho_\infty}{\gamma+1}\delta_\infty^2(\xi,\tau)-\frac{\gamma-1}{\gamma+1}p_\infty, \tag{55}$$

$$\rho(\xi,1,\tau)=\frac{\delta_\infty(\xi,\tau)}{\delta_S(\xi,\tau)}\rho_\infty, \tag{56}$$

where δ_S and δ_∞ are the component of fluid velocity normal to the shock in the shock-attached reference frame on the downstream and freestream sides of the shock, respectively, i.e.

$$\delta_S(\xi,\tau)=\begin{cases}\mathbf{v}\cdot\mathbf{e}_{\mathrm{SN}}|_{(\xi,1,\tau)}-v_{\mathrm{SN}}(\xi,\tau),\\ \mathbf{v}\cdot\mathbf{e}_{\mathrm{SN}}|_{(\xi,1,\tau)}-\left(\mathbf{e}_\eta\cdot\mathbf{e}_{\mathrm{SN}}\right)v(\xi,\tau),\end{cases} \tag{57}$$

$$\delta_\infty(\xi,\tau)=\mathbf{v}_\infty\cdot\mathbf{e}_{\mathrm{SN}}|_{(\xi,1,\tau)}-\left(\mathbf{e}_\eta\cdot\mathbf{e}_{\mathrm{SN}}\right)v(\xi,\tau), \tag{58}$$

and $\mathbf{v}(\xi,\eta,\tau)$ is the nondimensional velocity vector. The nondimensional freestream velocity vector $\mathbf{v}_\infty$ is

$$\mathbf{v}_\infty=\sqrt{\frac{\gamma p_\infty}{\rho_\infty}}M_\infty\mathbf{e}_z. \tag{59}$$

In Eqs. (53)–(57), $\mathbf{e}_{\mathrm{ST}}$ is a unit vector in the direction tangent to the shock wave, $\mathbf{e}_{\mathrm{SN}}$ is a unit vector in the direction normal to the shock wave, and $v_{\mathrm{SN}}(\xi,\tau)$ and $v(\xi,\tau)$ are the velocities of the shock in the $\mathbf{e}_{\mathrm{SN}}$ and $\mathbf{e}_\eta$ directions, respectively. Quantities denoted with a subscript of ∞ are freestream quantities, and those with no subscripts are post-shock quantities. The unit vectors $\mathbf{e}_{\mathrm{ST}}$ and $\mathbf{e}_{\mathrm{SN}}$ are in terms of the inverse metrics

$$\mathbf{e}_{\mathrm{ST}}=\left.\frac{-\frac{\partial\eta}{\partial z}\mathbf{e}_r+\frac{\partial\eta}{\partial r}\mathbf{e}_z}{\sqrt{\left(\frac{\partial\eta}{\partial z}\right)^2+\left(\frac{\partial\eta}{\partial r}\right)^2}}\right|_{(\xi,1,\tau)}, \tag{60}$$

$$\mathbf{e}_{\mathrm{SN}}=\left.\frac{\frac{\partial\eta}{\partial r}\mathbf{e}_r+\frac{\partial\eta}{\partial z}\mathbf{e}_z}{\sqrt{\left(\frac{\partial\eta}{\partial z}\right)^2+\left(\frac{\partial\eta}{\partial r}\right)^2}}\right|_{(\xi,1,\tau)}. \tag{61}$$

In order to solve the Rankine–Hugoniot equations, an expression for the shock velocity, $v(\xi,\tau)$, is needed. Differentiating Eqs. (54) and (55) with respect to time yields

$$\frac{\partial}{\partial\tau}\delta_S(\xi,\tau)=A_1(\xi,\tau)\frac{\partial}{\partial\tau}\delta_\infty(\xi,\tau), \tag{62}$$

$$\frac{\partial}{\partial\tau}p(\xi,1,\tau)=A_2(\xi,\tau)\frac{\partial}{\partial\tau}\delta_\infty(\xi,\tau), \tag{63}$$

where

$$A_1(\xi,\tau)=\frac{\gamma-1}{\gamma+1}-\frac{2\gamma}{(\gamma+1)\delta_\infty^2(\xi,\tau)},\quad A_2(\xi,\tau)=\frac{4\delta_\infty(\xi,\tau)}{\gamma+1}. \tag{64}$$

The terms $(\partial/\partial\tau)\delta_S(\xi,\tau)$ and $(\partial/\partial\tau)\delta_\infty(\xi,\tau)$ in Eqs. (62) and (63) are found by differentiating Eqs. (57) and (58), respectively, to yield the following:

$$\frac{\partial}{\partial\tau}\delta_S(\xi,\tau)=\left[\frac{\partial\mathbf{v}}{\partial\tau}\cdot\mathbf{e}_{\mathrm{SN}}+\mathbf{v}\cdot\frac{\partial\mathbf{e}_{\mathrm{SN}}}{\partial\tau}-\left(\mathbf{e}_\eta\cdot\mathbf{e}_{\mathrm{SN}}\right)\frac{\partial v}{\partial\tau}-v\mathbf{e}_\eta\cdot\frac{\partial\mathbf{e}_{\mathrm{SN}}}{\partial\tau}\right]\Bigg|_{(\xi,1,\tau)}, \tag{65}$$

$$\frac{\partial}{\partial\tau}\delta_\infty(\xi,\tau)=\left[\frac{\partial\mathbf{v}_\infty}{\partial\tau}\cdot\mathbf{e}_{\mathrm{SN}}+\mathbf{v}_\infty\cdot\frac{\partial\mathbf{e}_{\mathrm{SN}}}{\partial\tau}-\left(\mathbf{e}_\eta\cdot\mathbf{e}_{\mathrm{SN}}\right)\frac{\partial v}{\partial\tau}-v\mathbf{e}_\eta\cdot\frac{\partial\mathbf{e}_{\mathrm{SN}}}{\partial\tau}\right]\Bigg|_{(\xi,1,\tau)}. \tag{66}$$

Multiplying Eq. (62) by ρc and adding it to Eq. (63), and replacing the term $(\partial/\partial\tau)\delta_S(\xi,\tau)$ by Eq. (65) and the term $(\partial/\partial\tau)\delta_\infty(\xi,\tau)$ by (66), we arrive at the following equation for the shock acceleration $(\partial/\partial\tau)v(\xi,\tau)$,

$$\frac{\partial}{\partial\tau}v(\xi,\tau)=\left.\frac{\left[(A_2+\rho cA_1)\left(\mathbf{v}_\infty-v\mathbf{e}_\eta\right)-\rho c\left(\mathbf{v}-v\mathbf{e}_\eta\right)\right]\cdot\frac{\partial\mathbf{e}_{\mathrm{SN}}}{\partial\tau}-\rho c\frac{\partial\mathbf{v}}{\partial\tau}\cdot\mathbf{e}_{\mathrm{SN}}-\frac{\partial p}{\partial\tau}}{\left(\mathbf{e}_\eta\cdot\mathbf{e}_{\mathrm{SN}}\right)\left[A_2+\rho c(A_1-1)\right]}\right|_{(\xi,1,\tau)}. \tag{67}$$

The terms $\partial p/\partial\tau$ and $\rho c(\partial\mathbf{v}/\partial\tau)\cdot\mathbf{e}_{\mathrm{SN}}$ must be specified by a compatibility equation which is the characteristic equation associated with the wave propagating from the body to the shock along the normal direction. This compatibility equation is in the same form as the fourth compatibility equation in Eq. (46) only written in shock coordinates instead of the body coordinate system (ξ,η,τ). After some simplification, the following shock acceleration equation is obtained:

$$\frac{\partial}{\partial\tau}v(\xi,\tau)=\left.\frac{(A_2+\rho cA_1)\left(\mathbf{v}_\infty-v\mathbf{e}_\eta\right)\cdot\frac{\partial\mathbf{e}_{\mathrm{SN}}}{\partial\tau}-\rho c\left(\mathbf{v}-v\mathbf{e}_\eta\right)\cdot\frac{\partial\mathbf{e}_{\mathrm{SN}}}{\partial\tau}+A_3}{\left(\mathbf{e}_\eta\cdot\mathbf{e}_{\mathrm{SN}}\right)\left[A_2+\rho c(A_1-1)\right]}\right|_{(\xi,1,\tau)}, \tag{68}$$

where

$$\begin{aligned}A_3=&\,\widehat{u}\frac{\partial p}{\partial\xi}+\widehat{w}\frac{\partial p}{\partial\eta}+\gamma p\left(\frac{\partial\xi}{\partial z}\frac{\partial w}{\partial\xi}+\frac{\partial\eta}{\partial z}\frac{\partial w}{\partial\eta}+\frac{\partial\xi}{\partial r}\frac{\partial u}{\partial\xi}+\frac{\partial\eta}{\partial r}\frac{\partial u}{\partial\eta}\right)\\&+\rho c\left[\frac{\frac{\partial z}{\partial\xi}}{\sqrt{\left(\frac{\partial z}{\partial\xi}\right)^2+\left(\frac{\partial r}{\partial\xi}\right)^2}}\left(\widehat{u}\frac{\partial u_r}{\partial\xi}+\widehat{w}\frac{\partial u}{\partial\eta}+\frac{1}{\rho}\left(\frac{\partial\xi}{\partial r}\frac{\partial p}{\partial\xi}+\frac{\partial\eta}{\partial r}\frac{\partial p}{\partial\eta}\right)\right)\right.\\&\left.-\frac{\frac{\partial r}{\partial\xi}}{\sqrt{\left(\frac{\partial z}{\partial\xi}\right)^2+\left(\frac{\partial r}{\partial\xi}\right)^2}}\left(\widehat{u}\frac{\partial w}{\partial\xi}+\widehat{w}\frac{\partial w}{\partial\eta}+\frac{1}{\rho}\left(\frac{\partial\xi}{\partial z}\frac{\partial p}{\partial\xi}+\frac{\partial\eta}{\partial z}\frac{\partial p}{\partial\eta}\right)\right)\right]+\frac{\gamma pu}{r}.\end{aligned} \tag{69}$$

The time derivative of the normal unit vector, $\partial\mathbf{e}_{\mathrm{SN}}/\partial\tau$, is found by taking the time derivative of Eq. (61) with the metrics from Eq. (33) in place of the inverse metrics to yield

$$\frac{\partial\mathbf{e}_{\mathrm{SN}}}{\partial\tau}=\frac{\left(\frac{\partial r}{\partial\xi}\frac{\partial^2 z}{\partial\tau\,\partial\xi}-\frac{\partial z}{\partial\xi}\frac{\partial^2 r}{\partial\tau\,\partial\xi}\right)\left(\frac{\partial z}{\partial\xi}\mathbf{e}_z+\frac{\partial r}{\partial\xi}\mathbf{e}_r\right)}{\left(\left(\frac{\partial z}{\partial\xi}\right)^2+\left(\frac{\partial r}{\partial\xi}\right)^2\right)^{3/2}}. \tag{70}$$

Since there is a geometric singularity in Eq. (69) at $r=0$, the following alternate expression for $v(0,\tau)$ is employed

$$\frac{\partial}{\partial \xi} v(0,\tau) = 0. \tag{71}$$

We impose the following appropriate boundary conditions on the centerline, $\xi = 0$, in computational coordinates

$$\left.\frac{\partial w}{\partial \xi}\right|_{(0,\eta,\tau)} = 0, \tag{72}$$

$$\left.\frac{\partial p}{\partial \xi}\right|_{(0,\eta,\tau)} = 0, \tag{73}$$

$$u(0,\eta,\tau) = 0, \tag{74}$$

$$\rho(0,\eta,\tau) = \rho(0,1,\tau)\left(\frac{p(0,\eta,\tau)}{p(0,1,\tau)}\right)^{1/\gamma}. \tag{75}$$

The boundary condition in Eq. (75) comes from casting the energy equation, Eq. (18), in terms of the nondimensional entropy, s,

$$\frac{\partial s}{\partial t} + u\frac{\partial s}{\partial r} + w\frac{\partial s}{\partial z} = 0. \tag{76}$$

Enforcing steady state, $\partial s/\partial t = 0$, and zero velocity in the r direction, $u(0,\eta,\tau) = 0$, Eq. (76) reduces to $\frac{\partial s}{\partial z}|_{(0,\eta,\tau)} = 0$. Thus $s(0,\eta,\tau)$ is constant and equal to $s(0,1,\tau)$, the nondimensional value of the entropy downstream of the shock. Substituting $s(0,\eta,\tau) = \ln(p(0,1,\tau)/\rho(0,1,\tau)^{\gamma})$ into the equation for entropy, Eq. (24), and simplifying gives the boundary condition in Eq. (75). We note that the enforcement of steady state for entropy is artificial and potentially precludes some classes of unsteady behavior.

At the supersonic outflow boundary, $\xi = 1$, no physical boundary conditions are required as all waves are exiting the domain. Here the governing equations are solved in exactly the same manner as in the interior.

2.5. Summary of governing equations and boundary conditions

The governing equations and boundary conditions can be written in terms of the system of time-dependent partial differential and algebraic equations in Eqs. (2)–(4) in the two space dimensions, ξ and η, where

$$\mathbf{y}(\xi,\eta,\tau) = \begin{bmatrix} \rho(\xi,\eta,\tau) \\ u(\xi,\eta,\tau) \\ w(\xi,\eta,\tau) \\ p(\xi,\eta,\tau) \\ r(\xi,\eta,\tau) \\ z(\xi,\eta,\tau) \\ v_{\mathrm{BT}}(\xi,\tau) \\ \rho(\xi,0,\tau) \\ p(\xi,0,\tau) \\ v(\xi,\tau) \end{bmatrix}, \tag{77}$$

$$
\mathbf{f} = \left[
\begin{array}{ll}
-\widehat{u}\dfrac{\partial\rho}{\partial\xi} - \widehat{w}\dfrac{\partial\rho}{\partial\eta} - \rho\left(\dfrac{\partial\xi}{\partial r}\dfrac{\partial u}{\partial\xi} + \dfrac{\partial\xi}{\partial z}\dfrac{\partial w}{\partial\xi} + \dfrac{\partial\eta}{\partial r}\dfrac{\partial u}{\partial\eta} + \dfrac{\partial\eta}{\partial z}\dfrac{\partial w}{\partial\eta}\right) - \dfrac{\rho u}{r} & \text{Eq.(27)} \\
-\widehat{u}\dfrac{\partial u}{\partial\xi} - \widehat{w}\dfrac{\partial u}{\partial\eta} - \dfrac{1}{\rho}\left(\dfrac{\partial\xi}{\partial r}\dfrac{\partial p}{\partial\xi} + \dfrac{\partial\eta}{\partial r}\dfrac{\partial p}{\partial\eta}\right) & \text{Eq.(28)} \\
-\widehat{u}\dfrac{\partial w}{\partial\xi} - \widehat{w}\dfrac{\partial w}{\partial\eta} - \dfrac{1}{\rho}\left(\dfrac{\partial\xi}{\partial z}\dfrac{\partial p}{\partial\xi} + \dfrac{\partial\eta}{\partial z}\dfrac{\partial p}{\partial\eta}\right) & \text{Eq.(29)} \\
-\widehat{u}\dfrac{\partial p}{\partial\xi} - \widehat{w}\dfrac{\partial p}{\partial\eta} - \gamma p\left(\dfrac{\partial\xi}{\partial r}\dfrac{\partial u}{\partial\xi} + \dfrac{\partial\xi}{\partial z}\dfrac{\partial w}{\partial\xi} + \dfrac{\partial\eta}{\partial r}\dfrac{\partial u}{\partial\eta} + \dfrac{\partial\eta}{\partial z}\dfrac{\partial w}{\partial\eta}\right) - \dfrac{\gamma p u}{r} & \text{Eq.(30)} \\
\dfrac{\eta\dfrac{\partial Z(\xi)}{\partial\xi}v(\xi,\tau)}{\sqrt{\left(\dfrac{\partial R(\xi)}{\partial\xi}\right)^2 + \left(\dfrac{\partial Z(\xi)}{\partial\xi}\right)^2}} & \text{Eq.(38)} \\
-\dfrac{\eta\dfrac{\partial R(\xi)}{\partial\xi}v(\xi,\tau)}{\sqrt{\left(\dfrac{\partial R(\xi)}{\partial\xi}\right)^2 + \left(\dfrac{\partial Z(\xi)}{\partial\xi}\right)^2}} & \text{Eq.(39)} \\
-\left.\dfrac{\left[\widehat{u}\left(\dfrac{\partial\eta}{\partial r}\dfrac{\partial w}{\partial\xi} - \dfrac{\partial\eta}{\partial z}\dfrac{\partial u}{\partial\xi}\right) + \dfrac{1}{\rho}\left(\dfrac{\partial\eta}{\partial r}\dfrac{\partial\xi}{\partial z} - \dfrac{\partial\eta}{\partial z}\dfrac{\partial\xi}{\partial r}\right)\dfrac{\partial p}{\partial\xi}\right]}{\sqrt{\left(\dfrac{\partial\eta}{\partial z}\right)^2 + \left(\dfrac{\partial\eta}{\partial r}\right)^2}}\right|_{(\xi,0,\tau)} & \text{Eq.(50)} \\
\left.\left[-\dfrac{1}{c^2}\dfrac{\partial p}{\partial\tau} + \widehat{u}\left(\dfrac{\partial\rho}{\partial\xi} - \dfrac{1}{c^2}\dfrac{\partial p}{\partial\xi}\right)\right]\right|_{(\xi,0,\tau)} & \text{Eq.(49)} \\
-\left.\left[\dfrac{\rho c\widehat{u}\left(\dfrac{\partial\eta}{\partial r}\dfrac{\partial u}{\partial\xi} + \dfrac{\partial\eta}{\partial z}\dfrac{\partial w}{\partial\xi}\right) + c\left(\dfrac{\partial\eta}{\partial r}\dfrac{\partial\xi}{\partial r} + \dfrac{\partial\eta}{\partial z}\dfrac{\partial\xi}{\partial z}\right)\dfrac{\partial p}{\partial\xi}}{\sqrt{\left(\dfrac{\partial\eta}{\partial z}\right)^2 + \left(\dfrac{\partial\eta}{\partial r}\right)^2}}\right.\right. & \\
\quad -\rho c^2\left(\dfrac{\partial\xi}{\partial r}\dfrac{\partial u}{\partial\xi} + \dfrac{\partial\xi}{\partial z}\dfrac{\partial w}{\partial\xi} + \dfrac{\partial\eta}{\partial r}\dfrac{\partial u}{\partial\eta} + \dfrac{\partial\eta}{\partial z}\dfrac{\partial w}{\partial\eta}\right) & \text{Eq.(51)} \\
\left.\left. +c\sqrt{\left(\dfrac{\partial\eta}{\partial z}\right)^2 + \left(\dfrac{\partial\eta}{\partial r}\right)^2}\dfrac{\partial p}{\partial\eta} - \widehat{u}\dfrac{\partial p}{\partial\xi} - \dfrac{\rho c^2 u}{r}\right]\right|_{(\xi,0,\tau)} & \\
\left.\left[\dfrac{(A_2 + \rho cA_1)(\mathbf{v}_\infty - v\mathbf{e}_\eta)\cdot\dfrac{\partial\mathbf{e}_{SN}}{\partial\tau} - \rho c(\mathbf{v} - v\mathbf{e}_\eta)\cdot\dfrac{\partial\mathbf{e}_{SN}}{\partial\tau} + A_3}{(\mathbf{e}_\eta\cdot\mathbf{e}_{SN})[A_2 + \rho c(A_1 - 1)]}\right]\right|_{(\xi,1,\tau)} & \text{Eq.(68)}
\end{array}
\right], \tag{78}
$$

$$
\mathbf{g} = \begin{bmatrix}
\left[u - \dfrac{v_{\mathrm{BT}} \dfrac{\partial r}{\partial \xi}}{\sqrt{\left(\dfrac{\partial r}{\partial \xi}\right)^2 + \left(\dfrac{\partial z}{\partial \xi}\right)^2}} \right]\Bigg|_{(\xi,0,\tau)} \\
\left[w - \dfrac{v_{\mathrm{BT}} \dfrac{\partial z}{\partial \xi}}{\sqrt{\left(\dfrac{\partial r}{\partial \xi}\right)^2 + \left(\dfrac{\partial z}{\partial \xi}\right)^2}} \right]\Bigg|_{(\xi,0,\tau)}
\end{bmatrix} \quad \text{Eq.(52)} \\
\rho(\xi,1,\tau) - \dfrac{\delta_\infty(\xi,\tau)}{\delta_S(\xi,\tau)} \quad \text{Eq.(56)} \\
[\mathbf{v}_\infty \cdot \mathbf{e}_{\mathrm{ST}} - \mathbf{v} \cdot \mathbf{e}_{\mathrm{ST}}]|_{(\xi,1,\tau)} \quad \text{Eq.(53)} \\
\delta_S(\xi,\tau) - \dfrac{\gamma-1}{\gamma+1}\delta_\infty(\xi,\tau) + \dfrac{2\gamma p_\infty}{(\gamma+1)\rho_\infty \delta_\infty(\xi,\tau)} \quad \text{Eq.(54)} \\
p(\xi,1,\tau) - \dfrac{2\rho_\infty}{\gamma+1}\delta_\infty^2(\xi,\tau) - \dfrac{\gamma-1}{\gamma+1}p_\infty \quad \text{Eq.(55)} \\
\rho(0,\eta,\tau) - \rho(0,1,\tau)\left(\dfrac{p(0,\eta,\tau)}{p(0,1,\tau)}\right)^{1/\gamma} \quad \text{Eq.(75)} \\
u(0,\eta,\tau) \quad \text{Eq.(74)} \\
\left.\dfrac{\partial w}{\partial \xi}\right|_{(0,\eta,\tau)} \quad \text{Eq.(72)} \\
\left.\dfrac{\partial p}{\partial \xi}\right|_{(0,\eta,\tau)} \quad \text{Eq.(73)} \\
\left.\dfrac{\partial v}{\partial \xi}\right|_{(0,\tau)} \quad \text{Eq.(71)}
\end{bmatrix}. \tag{79}
$$

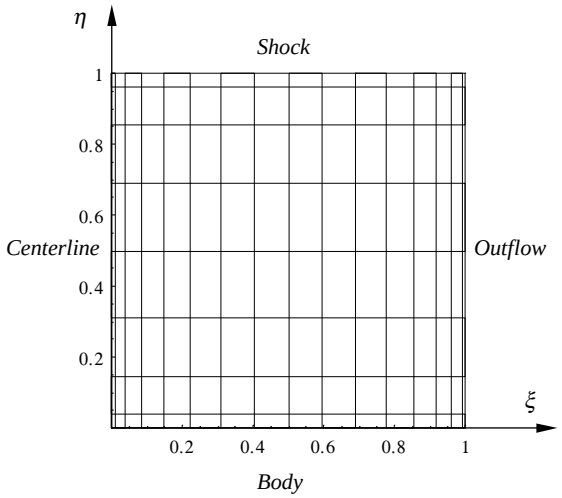

Fig. 2. Gauss–Lobatto Chebyshev computational grid for the shock-fitted blunt body.

In Eqs. (77)–(79) $\mathbf{y}(\xi,\eta,\tau):\mathbb{R}^3\rightarrow\mathbb{R}^{10}$ and $\mathbf{f}:\mathbb{R}^3\rightarrow\mathbb{R}^{10}$ while $\mathbf{g}:\mathbb{R}^3\rightarrow\mathbb{R}^{11}$. The functions $\mathbf{y}(\xi,\eta,\tau)$ and $\mathbf{f}$ contain six components which are time-dependent functions over the domain Ω with the remaining four components time-dependent functions defined for on S only. The equation $(\partial\mathbf{y}/\partial\tau)+\mathbf{f}=\mathbf{0}$ represents 10 partial differential equations with 10 unknowns and $\mathbf{g}=\mathbf{0}$ represents appropriate boundary conditions.

2.6. Numerical solution technique

In order to convert the system of partial differential and algebraic equations to a system of ODEs, it is necessary to approximate the spatial derivatives $\partial\mathbf{y}/\partial\xi$ and $\partial\mathbf{y}/\partial\eta$ at grid points (ξ_i,η_j), $i=0,\ldots,N$, $j=0,\ldots,M$. We choose to specify the grid in the computational domain, Fig. 2, according to the following Gauss–Lobatto Chebyshev distribution:

$$\begin{aligned}\xi_i&=\frac{1}{2}\left[1.-\cos\left(\frac{\pi}{N}i\right)\right],\quad i=0,\ldots,N,\\ \eta_j&=\frac{1}{2}\left[1.-\cos\left(\frac{\pi}{M}j\right)\right],\quad j=0,\ldots,M.\end{aligned}\tag{80}$$

This choice of nodes is not unique and is made because global Lagrange polynomial approximations of general nonperiodic functions defined on this grid were found in [29] to yield a more uniform and overall lower error than a uniform grid. The functions $\mathbf{y}(\xi,\eta,\tau)$ are approximated in terms of a double Lagrange global interpolating polynomial defined on the mesh ξ_n, $n=0,\ldots,N$, η_m, $m=0,\ldots,M$, i.e.

$$\mathbf{y}(\xi,\eta,\tau)\approx\sum_{n=0}^{N}\sum_{m=0}^{M}\mathbf{y}(\xi_n,\eta_m,\tau)L_n^{(N)}(\xi)L_m^{(M)}(\eta).\tag{81}$$

The Lagrange interpolating polynomials are

$$\begin{aligned}L_n^{(N)}(\xi)&=\frac{\prod_{l=0,\,l\neq n}^{N}(\xi-\xi_l)}{\prod_{l=0,\,l\neq n}^{N}(\xi_n-\xi_l)},\quad n=0,\ldots,N,\\ L_m^{(M)}(\eta)&=\frac{\prod_{l=0,\,l\neq m}^{M}(\eta-\eta_l)}{\prod_{l=0,\,l\neq m}^{M}(\eta_m-\eta_l)},\quad m=0,\ldots,M.\end{aligned}\tag{82}$$

It is easily shown that the Lagrange interpolating polynomials, $L_n^{(N)}(\xi)$ and $L_m^{(M)}(\eta)$, have the values of unity at $\xi=\xi_n$ and $\eta=\eta_m$ and zero at the other collocation points, i.e.

$$L_n^{(N)}(\xi_i)=\delta_{ni}=\begin{cases}0 & \text{if } n\neq i,\\ 1 & \text{if } n=i,\end{cases}\quad L_m^{(M)}(\eta_j)=\delta_{mj}=\begin{cases}0 & \text{if } m\neq j,\\ 1 & \text{if } m=j.\end{cases}\tag{83}$$

Derivatives of $\mathbf{y}(\xi,\eta,\tau;b)$ are evaluated by differentiating Eq. (81). Evaluating these derivatives on the grid, (ξ_i,η_j), chosen to be the same grid as that used to define the interpolating polynomial, i.e. $(\xi_i,\eta_j)\equiv(\xi_n,\eta_m)$, and making use of Eq. (83) yields

$$\begin{aligned}\left.\frac{\partial\mathbf{y}}{\partial\xi}\right|_{(\xi_i,\eta_j)}&\approx\sum_{n=0}^{N}\mathbf{y}(\xi_n,\eta_j,\tau)\frac{\mathrm{d}L_n}{\mathrm{d}\xi}(\xi_i),\\ \left.\frac{\partial\mathbf{y}}{\partial\eta}\right|_{(\xi_i,\eta_j)}&\approx\sum_{m=0}^{M}\mathbf{y}(\xi_i,\eta_m,\tau)\frac{\mathrm{d}L_m}{\mathrm{d}\eta}(\eta_j).\end{aligned}\tag{84}$$

The terms $(\mathrm{d}L_n/\mathrm{d}\xi)(\xi_i)$ and $(\mathrm{d}L_m/\mathrm{d}\eta)(\eta_j)$ in Eq. (84) are evaluated efficiently for an arbitrary grid using an algorithm developed by Fornberg [25]. The operation count for approximating the derivatives via Eq. (84) on an $N\times M$ grid is $(NM)^2$ operations for direct matrix multiplication used here. The points which both

define the Lagrange interpolating polynomials and at which derivatives are evaluated are chosen according to Eq. (80). The metrics $\partial^2 z/(\partial\tau\,\partial\xi)$ and $\partial^2 r/(\partial\tau\,\partial\xi)$ in Eq. (70) are specified by differentiating Eq. (84) with respect to time, i.e.

$$\begin{aligned}\frac{\partial^2 z(\xi_i,\eta_j,\tau)}{\partial\tau\,\partial\xi} &= \sum_{n=0}^{N}\frac{\partial}{\partial\tau}z(\xi_n,\eta_j,\tau)\frac{\mathrm{d}L_n}{\mathrm{d}\xi}(\xi_i),\\ \frac{\partial^2 r(\xi_i,\eta_j,\tau)}{\partial\tau\,\partial\xi} &= \sum_{n=0}^{N}\frac{\partial}{\partial\tau}r(\xi_n,\eta_j,\tau)\frac{\mathrm{d}L_n}{\mathrm{d}\xi}(\xi_i).\end{aligned} \tag{85}$$

After spatial discretization of Eqs. (77)–(79) on an $(N+1)\times(M+1)$ grid, the equations become a system of differential algebraic equations of the form in Eqs. (5) and (6) consisting of $P_2 = 6(NM+N+M)+5$ total equations and equal number of unknowns. The system is composed of $P_1 = 6NM+2M$ ODEs and $6N+4M+5$ algebraic equations, where the primary variables, $y_p(\tau)$, $p=1,\ldots,P_1$, taken to be those whose time derivative explicitly appears in Eq. (5) are

$$y_p(\tau) = \begin{bmatrix} \left.\begin{matrix}\rho(\xi_i,\eta_j,\tau)\\ u(\xi_i,\eta_j,\tau)\\ w(\xi_i,\eta_j,\tau)\\ p(\xi_i,\eta_j,\tau)\end{matrix}\right\} i=1,\ldots,N,\ j=1,\ldots,M-1,\\ \left.\begin{matrix}r(\xi_i,\eta_j,\tau)\\ z(\xi_i,\eta_j,\tau)\end{matrix}\right\} i=0,\ldots,N,\ j=1,\ldots,M,\\ \left.\begin{matrix}v_{\mathrm{BT}}(\xi_i,\tau)\\ \rho(\xi_i,0,\tau)\\ p(\xi_i,0,\tau)\\ v(\xi_i,\tau)\end{matrix}\right\} i=1,\ldots,N, \end{bmatrix}, \quad p=1,\ldots,P_1, \tag{86}$$

and the secondary variables $y_{p'}(\tau)$, $p'=P_1+1,\ldots,P_2$, are

$$y_{p'}(\tau) = \begin{bmatrix} \left.\begin{matrix}u(\xi_i,0,\tau)\\ w(\xi_i,0,\tau)\\ \rho(\xi_i,1,\tau)\\ u(\xi_i,1,\tau)\\ w(\xi_i,1,\tau)\\ p(\xi_i,1,\tau)\end{matrix}\right\} i=1,\ldots,N,\\ \left.\begin{matrix}\rho(0,\eta_j,\tau)\\ u(0,\eta_j,\tau)\\ w(0,\eta_j,\tau)\\ p(0,\eta_j,\tau)\end{matrix}\right\} j=0,\ldots,M,\\ v(0,\tau) \end{bmatrix}, \quad p'=P_1+1,\ldots,P_2. \tag{87}$$

The functions $f_p(y_1,\ldots,y_{P_2})$, $p=1,\ldots,P_1$, are

$$
f_p = \left[\begin{array}{l}
\left.\left[-\widehat{u}\dfrac{\partial\rho}{\partial\xi}-\widehat{w}\dfrac{\partial\rho}{\partial\eta}-\rho\left(\dfrac{\partial\xi}{\partial r}\dfrac{\partial u}{\partial\xi}+\dfrac{\partial\xi}{\partial z}\dfrac{\partial w}{\partial\xi}+\dfrac{\partial\eta}{\partial r}\dfrac{\partial u}{\partial\eta}+\dfrac{\partial\eta}{\partial z}\dfrac{\partial w}{\partial\eta}\right)-\dfrac{\rho u}{r}\right]\right|_{(\xi_i,\eta_j,\tau)} \\
\left.\left[-\widehat{u}\dfrac{\partial u}{\partial\xi}-\widehat{w}\dfrac{\partial u}{\partial\eta}-\dfrac{1}{\rho}\left(\dfrac{\partial\xi}{\partial r}\dfrac{\partial p}{\partial\xi}+\dfrac{\partial\eta}{\partial r}\dfrac{\partial p}{\partial\eta}\right)\right]\right|_{(\xi_i,\eta_j,\tau)} \\
\left.\left[-\widehat{u}\dfrac{\partial w}{\partial\xi}-\widehat{w}\dfrac{\partial w}{\partial\eta}-\dfrac{1}{\rho}\left(\dfrac{\partial\xi}{\partial z}\dfrac{\partial p}{\partial\xi}+\dfrac{\partial\eta}{\partial z}\dfrac{\partial p}{\partial\eta}\right)\right]\right|_{(\xi_i,\eta_j,\tau)} \\
\left.\left[-\widehat{u}\dfrac{\partial p}{\partial\xi}-\widehat{w}\dfrac{\partial p}{\partial\eta}-\gamma p\left(\dfrac{\partial\xi}{\partial r}\dfrac{\partial u}{\partial\xi}+\dfrac{\partial\xi}{\partial z}\dfrac{\partial w}{\partial\xi}+\dfrac{\partial\eta}{\partial r}\dfrac{\partial u}{\partial\eta}+\dfrac{\partial\eta}{\partial z}\dfrac{\partial w}{\partial\eta}\right)-\dfrac{\gamma p u}{r}\right]\right|_{(\xi_i,\eta_j,\tau)}
\end{array}\right\} i=1,\ldots,N,\ j=1,\ldots,M-1, \\
\left.\begin{array}{c}
\left.\dfrac{\eta\dfrac{\mathrm{d}Z(\xi)}{\mathrm{d}\xi}v(\xi,\tau)}{\sqrt{\left(\dfrac{\mathrm{d}R(\xi)}{\mathrm{d}\xi}\right)^2+\left(\dfrac{\mathrm{d}Z(\xi)}{\mathrm{d}\xi}\right)^2}}\right|_{(\xi_i,\eta_j,\tau)} \\
\left.-\dfrac{\eta\dfrac{\mathrm{d}R(\xi)}{\mathrm{d}\xi}v(\xi,\tau)}{\sqrt{\left(\dfrac{\mathrm{d}R(\xi)}{\mathrm{d}\xi}\right)^2+\left(\dfrac{\mathrm{d}Z(\xi)}{\mathrm{d}\xi}\right)^2}}\right|_{(\xi_i,\eta_j,\tau)}
\end{array}\right\} i=0,\ldots,N,\ j=1,\ldots,M, \\
\left.\begin{array}{l}
\left.-\dfrac{\left[\widehat{u}\left(\dfrac{\partial\eta}{\partial r}\dfrac{\partial w}{\partial\xi}-\dfrac{\partial\eta}{\partial z}\dfrac{\partial u}{\partial\xi}\right)+\dfrac{1}{\rho}\left(\dfrac{\partial\eta}{\partial r}\dfrac{\partial\xi}{\partial z}-\dfrac{\partial\eta}{\partial z}\dfrac{\partial\xi}{\partial r}\right)\dfrac{\partial p}{\partial\xi}\right]}{\sqrt{\left(\dfrac{\partial\eta}{\partial z}\right)^2+\left(\dfrac{\partial\eta}{\partial r}\right)^2}}\right|_{(\xi_i,0,\tau)} \\
\left.\left[-\dfrac{1}{c^2}\dfrac{\partial p}{\partial\tau}+\widehat{u}\left(\dfrac{\partial\rho}{\partial\xi}-\dfrac{1}{c^2}\dfrac{\partial p}{\partial\xi}\right)\right]\right|_{(\xi_i,0,\tau)} \\
\left.-\left[\dfrac{\rho c\widehat{u}\left(\dfrac{\partial\eta}{\partial r}\dfrac{\partial u}{\partial\xi}+\dfrac{\partial\eta}{\partial z}\dfrac{\partial w}{\partial\xi}\right)+c\left(\dfrac{\partial\eta}{\partial r}\dfrac{\partial\xi}{\partial r}+\dfrac{\partial\eta}{\partial z}\dfrac{\partial\xi}{\partial z}\right)\dfrac{\partial p}{\partial\xi}}{\sqrt{\left(\dfrac{\partial\eta}{\partial z}\right)^2+\left(\dfrac{\partial\eta}{\partial r}\right)^2}}\right.\right. \\
\qquad -\rho c^2\left(\dfrac{\partial\xi}{\partial r}\dfrac{\partial u}{\partial\xi}+\dfrac{\partial\xi}{\partial z}\dfrac{\partial w}{\partial\xi}+\dfrac{\partial\eta}{\partial r}\dfrac{\partial u}{\partial\eta}+\dfrac{\partial\eta}{\partial z}\dfrac{\partial w}{\partial\eta}\right) \\
\left.\left.+c\sqrt{\left(\dfrac{\partial\eta}{\partial z}\right)^2+\left(\dfrac{\partial\eta}{\partial r}\right)^2}\dfrac{\partial p}{\partial\eta}-\widehat{u}\dfrac{\partial p}{\partial\xi}-\dfrac{\rho c^2 u}{r}\right]\right|_{(\xi_i,0,\tau)} \\
\left.-\left[\dfrac{(A_2+\rho cA_1)(\mathbf{v}_\infty-v\mathbf{e}_\eta)\cdot\dfrac{\partial\mathbf{e}_{\mathrm{SN}}}{\partial\tau}-\rho c(\mathbf{v}-v\mathbf{e}_\eta)\cdot\dfrac{\partial\mathbf{e}_{\mathrm{SN}}}{\partial\tau}+A_3}{(\mathbf{e}_\eta\cdot\mathbf{e}_N)[A_2+\rho c(A_1-1)]}\right]\right|_{(\xi_i,1,\tau)}
\end{array}\right\} i=1,\ldots,N,
\end{array}\right] \tag{88}
$$

and the functions $g_{p'}(y_1,\ldots,y_{P_2})$, $p'=P_1+1,\ldots,P_2$, are

$$g_{p'}=\left[\begin{array}{c}
\left.\left[u-\dfrac{v_{\mathrm{BT}}\dfrac{\partial r}{\partial\xi}}{\sqrt{\left(\dfrac{\partial r}{\partial\xi}\right)^2+\left(\dfrac{\partial z}{\partial\xi}\right)^2}}\right]\right|_{(\xi_i,0,\tau)} \\
\left.\left[w-\dfrac{v_{\mathrm{BT}}\dfrac{\partial z}{\partial\xi}}{\sqrt{\left(\dfrac{\partial r}{\partial\xi}\right)^2+\left(\dfrac{\partial z}{\partial\xi}\right)^2}}\right]\right|_{(\xi_i,0,\tau)} \\
\rho(\xi_i,1,\tau)-\dfrac{\delta_\infty(\xi_i,\tau)}{\delta_S(\xi_i,\tau)}\rho_\infty \\
\left[\mathbf{v}_\infty\cdot\mathbf{e}_{\mathrm{ST}}-\mathbf{v}\cdot\mathbf{e}_{\mathrm{ST}}\right]|_{(\xi_i,1,\tau)} \\
\delta_S(\xi_i,\tau)-\dfrac{\gamma-1}{\gamma+1}\delta_\infty(\xi_i,\tau)+\dfrac{2\gamma p_\infty}{(\gamma+1)\rho_\infty\delta_\infty(\xi_i,\tau)} \\
p(\xi_i,1,\tau)-\dfrac{2\rho_\infty}{\gamma+1}\delta_\infty^2(\xi_i,\tau)-\dfrac{\gamma-1}{\gamma+1}p_\infty
\end{array}\right\}\ i=1,\ldots,N,$$

$$\left.\begin{array}{c}
\rho\left(0,\eta_j,\tau\right)-\rho(0,1,\tau)\left(\dfrac{p\left(0,\eta_j,\tau\right)}{p(0,1,\tau)}\right)^{1/\gamma} \\
u\left(0,\eta_j,\tau\right) \\
\left.\dfrac{\partial w}{\partial\xi}\right|_{\left(0,\eta_j,\tau\right)} \\
\left.\dfrac{\partial p}{\partial\xi}\right|_{\left(0,\eta_j,\tau\right)}
\end{array}\right\}\ j=0,\ldots,M,$$

$$\left.\begin{array}{c}
\dfrac{\partial}{\partial\xi}v(0,\tau)
\end{array}\right] \tag{89}$$

There are no equations for the grid points on the body since these are fixed in time, nor is there an equation for the tangential velocity on the body at the centerline since this quantity is redundant, the velocity components, $u(0,\eta_j,\tau)$, $w(0,\eta_j,\tau)$, already being specified by Eqs. (72) and (74).

Finally, the secondary variables $y_{p'}$, $p'=P_1+1,\ldots,P_2$, in Eq. (89) are solved for explicitly in terms of the primary variables y_p, $p=1,\ldots,P_1$. Making use of Eq. (84) yields the following expression for $w(0,\eta_j,\tau)$,

$$w\left(0,\eta_j,\tau\right)=\frac{\sum_{n=1}^{N}w(\xi_n,\eta_j,\tau)\frac{\mathrm{d}L_n}{\mathrm{d}\xi}(0)}{\frac{\mathrm{d}L_0}{\mathrm{d}\xi}(0)}; \tag{90}$$

similar expressions are found for $p(0,\eta_j,\tau)$, and $v(0,\tau)$. Eqs. (53) and (54) are reformulated into the following two equations for the quantities $u(\xi_i,1,\tau)$ and $w(\xi_i,1,\tau)$, $i=1,\ldots,N$,

$$
\begin{aligned}
u(\xi_i,1,\tau) &= \left[\frac{\frac{\partial z}{\partial \xi}\frac{\partial r}{\partial \xi}\sqrt{\gamma}M_\infty}{\left(\frac{\partial z}{\partial \xi}\right)^2+\left(\frac{\partial r}{\partial \xi}\right)^2}+\frac{\frac{\partial z}{\partial \xi}\left[\delta+\left(\mathbf{e}_\eta\cdot\mathbf{e}_{\mathrm{SN}}\right)v\right]}{\sqrt{\left(\frac{\partial z}{\partial \xi}\right)^2+\left(\frac{\partial r}{\partial \xi}\right)^2}}\right]\Bigg|_{(\xi_i,1,\tau)},\\
w(\xi_i,1,\tau) &= \left[\frac{\left(\frac{\partial z}{\partial \xi}\right)^2\sqrt{\gamma}M_\infty}{\left(\frac{\partial z}{\partial \xi}\right)^2+\left(\frac{\partial r}{\partial \xi}\right)^2}-\frac{\frac{\partial r}{\partial \xi}\left[\delta+\left(\mathbf{e}_\eta\cdot\mathbf{e}_{\mathrm{SN}}\right)v\right]}{\sqrt{\left(\frac{\partial z}{\partial \xi}\right)^2+\left(\frac{\partial r}{\partial \xi}\right)^2}}\right]\Bigg|_{(\xi_i,1,\tau)}.
\end{aligned}
\tag{91}
$$

Once the quantities $w(0,\eta_j,\tau)$, $p(0,\eta_j,\tau)$, $z(0,\eta_j,\tau)$, and $v(0,\tau)$ are found from Eq. (90) and $u(\xi_i,1,\tau)$ and $w(\xi_i,1,\tau)$ are found from Eq. (91), the algebraic equations, $g_{p'}(y_1,\ldots,y_{P_2})$, Eq. (89), are written in the form of Eq. (8) where

$$
\widehat{g}_{p'} = \left[\begin{array}{c}
\left[\dfrac{v_{\mathrm{BT}}\frac{\partial r}{\partial \xi}}{\sqrt{\left(\frac{\partial r}{\partial \xi}\right)^2+\left(\frac{\partial z}{\partial \xi}\right)^2}}\right]\Bigg|_{(\xi_i,0,\tau)}\\
\left[\dfrac{v_{\mathrm{BT}}\frac{\partial z}{\partial \xi}}{\sqrt{\left(\frac{\partial r}{\partial \xi}\right)^2+\left(\frac{\partial z}{\partial \xi}\right)^2}}\right]\Bigg|_{(\xi_i,0,\tau)}\\
\dfrac{\delta_\infty(\xi_i,\tau)}{\delta_S(\xi_i,\tau)}\rho_\infty\\
\left[\dfrac{\frac{\partial z}{\partial \xi}\frac{\partial r}{\partial \xi}\sqrt{\gamma}M_\infty}{\left(\frac{\partial z}{\partial \xi}\right)^2+\left(\frac{\partial r}{\partial \xi}\right)^2}+\dfrac{\frac{\partial z}{\partial \xi}\left[\delta_S+\left(\mathbf{e}_\eta\cdot\mathbf{e}_{\mathrm{SN}}\right)v\right]}{\sqrt{\left(\frac{\partial z}{\partial \xi}\right)^2+\left(\frac{\partial r}{\partial \xi}\right)^2}}\right]\Bigg|_{(\xi_i,1,\tau)}\\
\left[\dfrac{\left(\frac{\partial z}{\partial \xi}\right)^2\sqrt{\gamma}M_\infty}{\left(\frac{\partial z}{\partial \xi}\right)^2+\left(\frac{\partial r}{\partial \xi}\right)^2}-\dfrac{\frac{\partial r}{\partial \xi}\left[\delta_S+\left(\mathbf{e}_\eta\cdot\mathbf{e}_{\mathrm{SN}}\right)v\right]}{\sqrt{\left(\frac{\partial z}{\partial \xi}\right)^2+\left(\frac{\partial r}{\partial \xi}\right)^2}}\right]\Bigg|_{(\xi_i,1,\tau)}\\
\dfrac{2\rho_\infty}{\gamma+1}\delta_\infty^2(\xi_i,\tau)+\dfrac{\gamma-1}{\gamma+1}p_\infty
\end{array}\right\} i=1,\ldots,N,
\left[\begin{array}{c}
\left[\rho(0,1,\tau)\left(\dfrac{\sum_{n=1}^{N}p(\xi_n,\eta_j,\tau)\frac{\mathrm{d}L_n}{\mathrm{d}\xi}(0)}{p(0,1,\tau)\frac{\mathrm{d}L_0}{\mathrm{d}\xi}(0)}\right)^{1/\gamma}\right]\Bigg|_{(0,\eta_j,\tau)}\\
0\\
\dfrac{\sum_{n=1}^{N}w(\xi_n,\eta_j,\tau)\frac{\mathrm{d}L_n}{\mathrm{d}\xi}(0)}{\frac{\mathrm{d}L_0}{\mathrm{d}\xi}(0)}\\
\dfrac{\sum_{n=1}^{N}p(\xi_n,\eta_j,\tau)\frac{\mathrm{d}L_n}{\mathrm{d}\xi}(0)}{\frac{\mathrm{d}L_0}{\mathrm{d}\xi}(0)}\\
\dfrac{\sum_{n=1}^{N}v(\xi_n,\tau)\frac{\mathrm{d}L_n}{\mathrm{d}\xi}(0)}{\frac{\mathrm{d}L_0}{\mathrm{d}\xi}(0)}
\end{array}\right\} j=0,\ldots,M,
\tag{92}
$$

and $\delta_S(\xi_i,\tau) = ((\gamma-1)/(\gamma+1))\delta_\infty(\xi_i,\tau) - 2\gamma p_\infty/((\gamma+1)\rho_\infty\delta_\infty(\xi_i,\tau))$.

The initial conditions for the shock distance, $h(\xi_i,\tau)$, are taken to be constant, i.e., $h(\xi_i,\tau) = h(0,\tau) = 0.25$, $i = 1,\ldots,N$, which is sufficient to set initial conditions for the remainder of the physical grid coordinates, $r(\xi_i,\eta_j,\tau)$, $z(\xi_i,\eta_j,\tau)$, $i = 0,\ldots,N$, $j = 0,\ldots,M$, by making use of Eqs. (34) and (35). The shock velocity, $v(\xi_i,\tau)$, $i = 0,\ldots,N$, is initially set to zero. The initial values for the variables, $\rho(\xi_i,\eta_j,\tau)$, $u(\xi_i,\eta_j,\tau)$, $w(\xi_i,\eta_j,\tau)$, $p(\xi_i,\eta_j,\tau)$, $i = 1,\ldots,N$, $j = 1,\ldots,M$, $\rho(\xi_i,0,\tau)$, $u(\xi_i,0,\tau)$, and $p(\xi_i,0,\tau)$, $i = 1,\ldots,N$, are set equal to the value behind the shock at $(\eta = 1)$ for the corresponding ξ coordinate line, e.g. $\rho(\xi_i,\eta_j,0) = \rho(\xi_i,1,0)$. The initial values for $u(\xi_i,0,\tau)$, $i = 1,\ldots,N$, are chosen so that the boundary condition at $\eta = 0$, Eq. (41) is satisfied exactly, and the initial values for $\rho(0,\eta_j,\tau)$, $u(0,\eta_j,\tau)$, $w(0,\eta_j,\tau)$, $p(0,\eta_j,\tau)$, $j = 0,\ldots,M$, are chosen so that the boundary conditions at $\xi = 0$, Eqs. (72)–(75) are satisfied exactly. The initial values for the variables $v_{\mathrm{BT}}(\xi_i,\tau)$, $i = 1,\ldots,N$, are prescribed once the values for $r(\xi_i,0,\tau)$, $z(\xi_i,0,\tau)$, $u(\xi_i,0,\tau)$ and $w(\xi_i,0,\tau)$ have been specified.

Solutions have been obtained for the system of ODEs, Eqs. (9), with the standard ODE solver LSODA, [30,31], which automatically adjusts the time step to achieve a specified level of accuracy. It also automatically switches between an explicit method and implicit method depending on the stiffness of the problem. A typical steady state calculation on a 17×9 grid took 106 s CPU time on a single 800 MHz processor with 512 MB of RAM. For the steady state problems, the criteria for stopping the integration is when the $L_\infty[\Omega]$ error in $\rho(\xi,\eta,\tau\to\infty)$ does not change appreciably. Finally, since LSODA automatically switches between an explicit method and implicit method depending, it may be of interest to note that early in the calculation, less than 10% of LSODA's time steps were implicit whereas about 50% of the time steps were run in implicit mode as the calculations neared steady state. Apparently as the level of error approached the level of the discretization error, the problem became increasingly stiff causing LSODA to switch to implicit mode.

2.7. Pseudospectral flow solver verification and validation

2.7.1. Taylor–Maccoll solution

The solution to supersonic flow over a cone, also known as the Taylor–Maccoll solution [32], will be used to verify the code described in the previous section. We first use a highly accurate ODE solver to calculate the Taylor–Maccoll solution, which we will subsequently refer to as the exact solution. The only modification to the blunt body problem formulation to generate numerical approximations to the Taylor–Maccoll flow is to replace the centerline boundary condition at $\xi = 0$ with a Dirichlet boundary condition containing the values of ρ, u, w, p, r, and z taken from the exact solution. A schematic of a 40° cone including the physical and computational coordinates is shown in Fig. 3 for a 5×5 grid for $M_\infty = 3.5$, $\rho_\infty = p_\infty = 1$. A value of $r_0 = 0.1$ was chosen for the results presented in this section. The initial conditions for ρ, u, w, p, r, and z are taken from the exact solution, and a sinusoidal distribution is chosen for the initial shock velocity, i.e. $v(\xi,0) = 0.1\sin(2\pi\xi)$. In Fig. 4, we show the time history of the $L_\infty[\Omega]$ error in $\rho(\xi,\eta)$ over the domain, Ω, for the pseudospectral prediction measured against the exact solution for a $M_\infty = 3.5$ flow over a 40° cone solved on a 5×17 grid. The figure demonstrates a rapid relaxation to the exact solution.

A grid convergence test for the pseudospectral prediction of the Taylor–Maccoll flow is conducted by refining the grid in the η-direction for a fixed number of 5 nodes in the ξ-direction. The accuracy of the method is unaffected by grid refinement in the ξ-direction since all derivatives are zero in that direction. As we can see from Fig. 5, there is a rapid decrease in the error until about 10^{-12} when the error flattens probably due to roundoff error. Note the spectral nature of the grid convergence, that is the slope of the error curve continues to steepen with increasing number of nodes, at least until the roundoff limit is reached, and does not reach a constant value for the slope as would be the case for a method with a fixed order of accuracy.

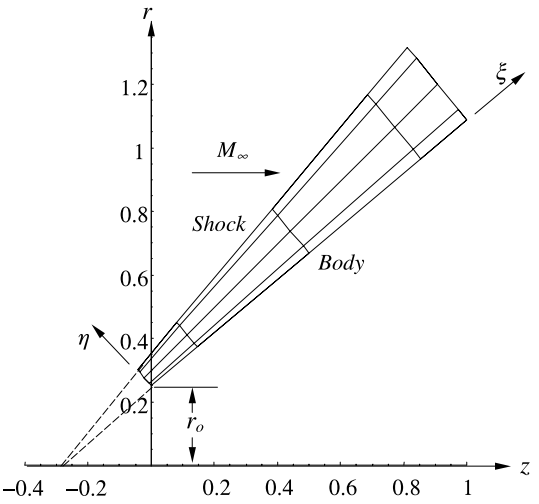

Fig. 3. Schematic of the physical (r,z) and computational (ξ,η) grids for the Taylor–Maccoll problem.

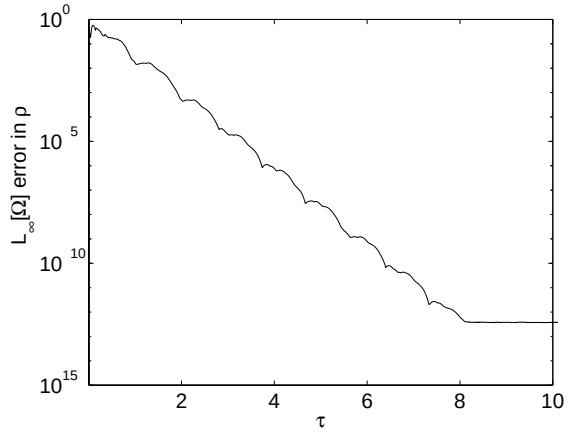

Fig. 4. Single 5×17 grid $L_\infty[\Omega]$ residual error in $\rho(\xi,\eta)$ measured against Taylor–Maccoll similarity solution as a function of time, τ, for a 40° cone at $M_\infty = 3.5$.

2.7.2. Steady state blunt body results

The following functions have been chosen to parameterize the blunt body surface

$$R(\xi) = \xi, \tag{93}$$

$$Z(\xi) = \xi^{1/b}, \tag{94}$$

where the domain for the geometric parameter b is restricted to $b \in (0,1)$. Eliminating the parameter ξ, we see that the body surface is described by $R = Z^b$. For $b = 0.5$, $M_\infty = 3.5$, $\rho_\infty = p_\infty = 1$, contour plots of Mach number and pressure are shown in Figs. 6 and 7. The sonic line, $M = 1$, is predicted in Fig. 6 as well as the fact that the outflow velocity is indeed supersonic as required in the derivation of the outflow

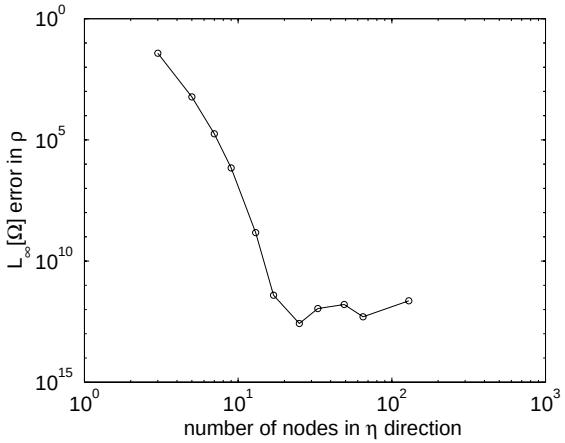

Fig. 5. $L_\infty[\Omega]$ error in $\rho(\xi,\eta)$ measured against a Taylor–Maccoll similarity solution for a 40° cone in $M_\infty = 3.5$ flow as grid is refined in the η direction.

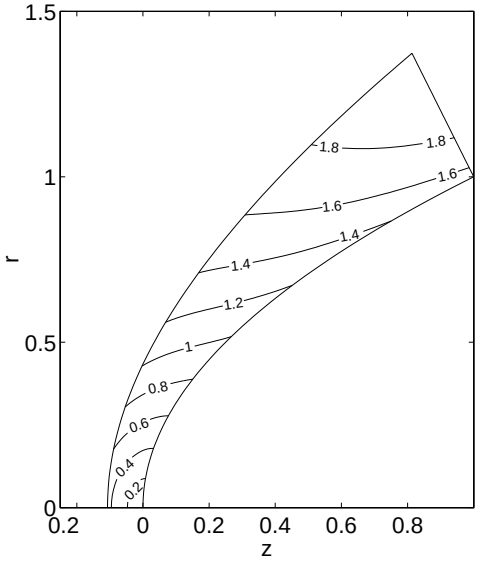

Fig. 6. Contours of Mach number for flow over the blunt body for $b = 0.5$, $M_\infty = 3.5$, 17×9 grid.

boundary condition. In Fig. 7, the pressure at the stagnation point is seen to be more than 16 times the freestream pressure at $M_\infty = 3.5$, and the jump in pressure across the normal shock at the centerline is over 13 times the freestream pressure.

As a means of code validation, a comparison is made between the numerical results for the pressure distribution on the body with that of the modified Newtonian [33] sine squared law

$$C_\mathrm{p} = C_{\mathrm{p}0} \sin^2 \phi, \tag{95}$$

where $C_{\mathrm{p}0}$ is the pressure coefficient at the body stagnation point and ϕ is the local surface inclination angle measured with respect to the z axis. The pressure coefficient, C_p, is defined as

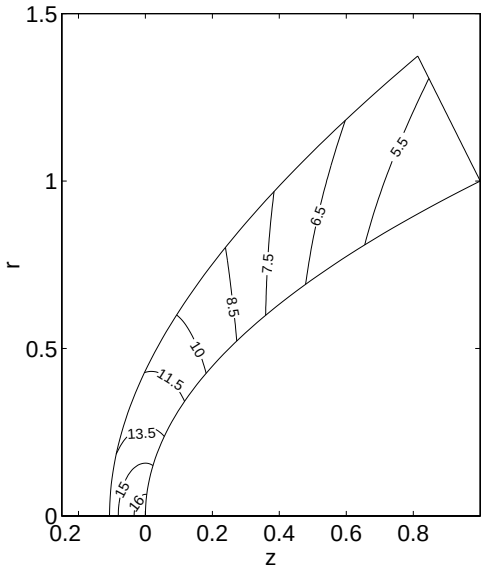

Fig. 7. Contours of pressure for flow over the blunt body for $b = 0.5$, $M_\infty = 3.5$, 17×9 grid.

$$C_p = \frac{p^* - p^*_\infty}{\frac{1}{2}\rho^*_\infty w^{*2}_\infty} = \frac{p(\xi, 0, \tau) - 1}{\frac{1}{2}\gamma M^2_\infty}. \tag{96}$$

The modified Newtonian approximation is a semi-analytical model for the surface pressure distribution over blunt bodies. Anderson [34] reports that for a power law body with $b = 0.5$ and aspect ratio near unity, the modified Newtonian approximation does well in predicting the pressure distribution on the surface of the body. As can be seen from Fig. 8, the pseudospectral code also predicts close agreement for the pressure

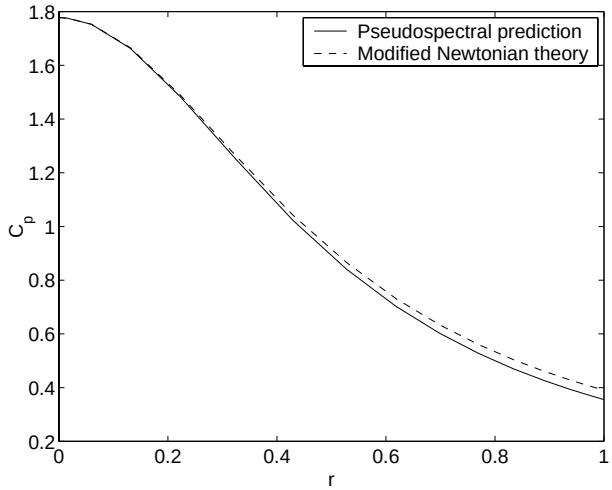

Fig. 8. Blunt body surface C_p distribution predictions at $M_\infty = 3.5$ from modified Newtonian theory and from the pseudospectral method, where $b = 0.5$; 17×9 grid.

distribution on the surface of the body defined by $r = \sqrt{z}$. As a further check on the validity of the pseudospectral code in Fig. 9 a comparison is made of the pseudospectral prediction for the shock shape for $M_\infty = 3.5$ flow over a sphere with that of an empirical formula by Billig [35] developed for flow over spherically blunted cones based on experiment.

A grid convergence study is performed for the blunt body with the $L_\infty[\Omega]$ error over the domain, Ω in $\rho(\xi,\eta)$ shown in Fig. 10, at $M_\infty = 3.5$ and $b = 0.5$, where the error is measured against a 65×33 or 2145 node numerical solution. For 861 nodes, the $L_\infty[\Omega]$ error over the domain, Ω in $\rho(\xi,\eta)$, has been reduced to the order of 10^{-12} and subsequently flattens due to roundoff error. Like grid convergence plots for the Taylor–Maccoll solution, the convergence of the error for the blunt body problem shows a spectral convergence rate as expected of the pseudospectral numerical technique.

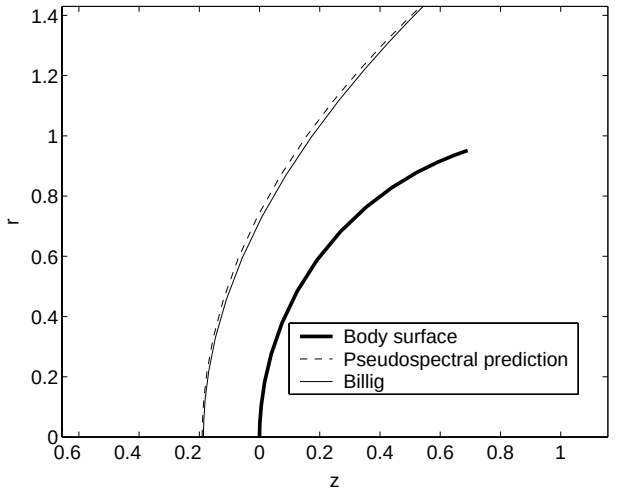

Fig. 9. Shock shape prediction of the pseudospectral code for a sphere $M_\infty = 3.5$ compared with an empirical formula by Billig [35] derived from experiments; 17×9 grid.

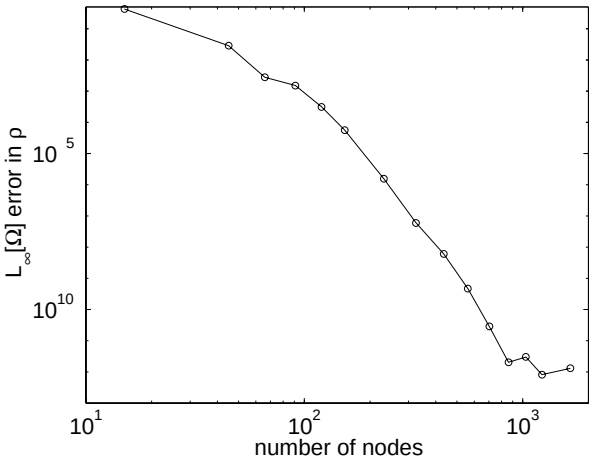

Fig. 10. Grid convergence $L_\infty[\Omega]$ error in $\rho(\xi,\eta)$ measured against a baseline, 65×33 grid, solution for a $b = 0.5$, $M_\infty = 3.5$ blunt body.

2.7.3. Unsteady acoustic wave interaction with attached shock

Now we turn to a fundamentally unsteady problem: the interaction of an unsteady, planar acoustic wave with an attached shock, for which the automatic time step selection in LSODA enables us to have tight control over the error in the solution. A schematic of the grid is shown in Fig. 3, where $r_0 = 0.01$ is chosen for this problem. The values of the freestream flow quantities ρ_∞, u_∞, w_∞, p_∞ at the shock are taken to be

$$\rho_\infty = -\frac{1}{2\sqrt{\gamma}}(F(\xi,\tau) - G(\xi,\tau)), \tag{97}$$

$$u_\infty = 0, \tag{98}$$

$$w_\infty = \frac{1}{2}(F(\xi,\tau) + G(\xi,\tau)), \tag{99}$$

$$p_\infty = 1 + \gamma(\rho_\infty - 1), \tag{100}$$

where

$$F(\xi,\tau) = \sqrt{\gamma}(M_\infty - 1), \tag{101}$$

$$G(\xi,\tau) = \sqrt{\gamma}(M_\infty + 1)(1 + \epsilon \sin\kappa(z(\xi,1,\tau) - \sqrt{\gamma}(M_\infty + 1)\tau)). \tag{102}$$

Choosing $\epsilon = 0.01$, $\kappa = 6\pi$, $M_\infty = 3.5$, and $\gamma = 1.4$ in Eqs. (101) and (102), the system of ODEs in Eq. (9) are integrated in time for $\tau \in [0,2]$ on a 33×17 grid using the ODE solver LSODA. The CPU time for the calculation on a single 800 MHz processor was 7.5 h. The initial conditions were set to the Taylor–Maccoll solution of the unperturbed freestream flow conditions, i.e. $\rho_\infty = 1$, $u_\infty = 0$, $w_\infty = \sqrt{\gamma}M_\infty$, $p_\infty = 1$. The relative and absolute error tolerances for the time integration were set to 10^{-10} and 10^{-12}, respectively, in LSODA. As an estimate for the spatial accuracy, we recall that the $L_\infty[\Omega]$ error in $\rho(\xi,\eta)$ on a 33×17 grid for the steady state calculations was 10^{-12} and 10^{-9} for the Taylor–Maccoll and blunt body flows, respectively.

Let us analyze the motion of a single point on the shock located at $\xi = \eta = 1$. The power spectrum, $P(f)$, as a function of reduced frequency for the perturbation in freestream density, $\Delta\rho_\infty = \rho_\infty - 1$, and shock distance function, $\Delta h = h(1,t) - h_\infty(1)$, at the point $\xi = \eta = 1$ are presented in Fig. 11 as well as $\Delta\rho_\infty|_{z=-1}$, which is well upstream of the shock. Initial transients in the solution are neglected in the estimation of the power spectrum by considering only $\tau \in [1.001, 2]$, so that the time interval is $T = 0.999$. The power spectrum is defined at $K/2 + 1$ frequencies as

$$\begin{aligned} P(f_0) &= \frac{1}{K^2}|C_0|^2, \\ P(f_k) &= \frac{1}{K^2}\left[|C_k|^2 + |C_{K-k}|^2\right], \quad k = 1, \ldots, \left(\frac{K}{2} - 1\right), \\ P(f_{K/2}) &= \frac{1}{K^2}|C_{K/2}|^2, \end{aligned} \tag{103}$$

where f_k is defined only for the zero and positive frequencies

$$f_k = \frac{k}{K\Delta}, \quad k = 0, \ldots, \left(\frac{K}{2}\right), \tag{104}$$

where $\Delta = 0.001$ is the chosen sampling interval, $K = T/\Delta + 1 = 1000$ is the number of sampled points, and the C_k are the discrete Fourier coefficients. The power spectrum, Fig. 11, clearly shows a large peak in the

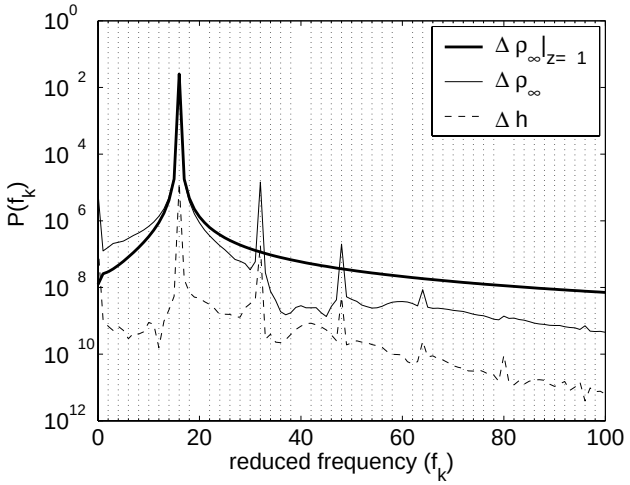

Fig. 11. Frequency spectrum at a single point on the shock ($\xi = 1$) of the fluctuations in freestream density, $\Delta\rho_\infty = \rho_\infty - 1$, and the response of the shock, $\Delta h = h(1,t) - h_\infty(1)$. $M_\infty = 3.5$; 33×17 grid.

power spectrum for $\Delta\rho_\infty|_{z=-1}$ at a reduced frequency of $f_{16} = (\kappa/2\pi)\sqrt{\gamma}(M_\infty + 1) = 16.0$, according to Eq. (9). Peaks in the power spectrum of Δh, and $\Delta\rho_\infty$ also appear at $f_{16} = 16.0$ in response to the frequency of oscillation of $\Delta\rho_\infty|_{z=-1}$. In addition, higher harmonics at integer multiples of the $f_{16} = 16.0$ 'forcing' frequency are present in the power spectrum of Δh and $\Delta\rho_\infty$.

The time history of the density fluctuations and perturbation in shock distance function both measured at the point $\xi = \eta = 1$ are shown in Fig. 12 for $\tau \in [1.75, 2.0]$. It is evident from Fig. 12 that the freestream density fluctuations are nearly 180° out of phase with the shock distance perturbations, and that the amplitude of the density fluctuations are 20% of the mean flow, while the shock response is two orders of magnitude below the perturbations in freestream density. The high accuracy of the current method is critical in capturing the correct shock dynamics for such small amplitude fluctuations, and in predicting the higher harmonics of the shock fluctuations in Fig. 11, where the amplitude of the power spectrum drops

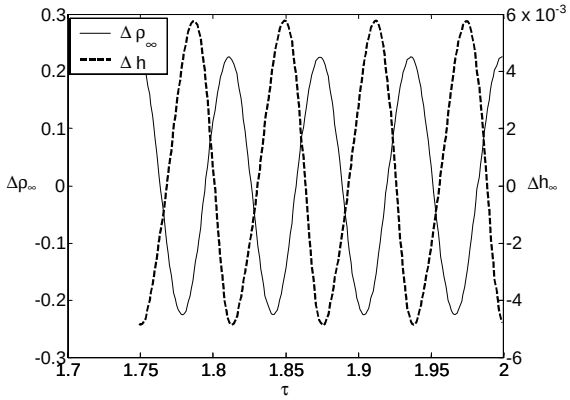

Fig. 12. Time history at a single point on the shock ($\xi = 1$) of the fluctuations in freestream density, $\Delta\rho_\infty = \rho_\infty - 1$, and the response of the shock, $\Delta h = h(1,t) - h_\infty(1)$. $M_\infty = 3.5$; 33×17 grid.

several orders of magnitude with each successively increasing harmonic. The current method is able to resolve up to the fourth harmonic of Δh, whose amplitude in the power spectrum is on the order of 10^{-10}.

3. Conclusion

In this study, we have described a pseudospectral numerical approximation technique for the inviscid supersonic flow over a blunt body geometry in which the discretized form of the governing equations and boundary conditions are formulated in terms of a system of ODE's which can be solved using a standard ODE solver. This formulation leverages the strengths of widely available ODE solvers to generate time accurate solutions within prescribed error tolerances through automatic time step selection and explicit/implicit switching. Additionally, fitting of the shock and the use of global polynomials in the solution approximation permit high accuracy steady state approximations with 10^{-5} error in as little as 106 s on a single 800 MHz processor. Even higher accuracy has been achieved for a time-dependent problem. This standard formulation has important potential applications such as approximating unsteady shock phenomena with sufficient accuracy to discern between physical versus numerical instabilities.

References

[1] G.P. Brooks, J.M. Powers, A Karhunen-Loève least-squares technique for optimization of geometry of a blunt body in supersonic flow, J. Comput. Phys. (2004), in press.
[2] D. Gottlieb, S. Orszag, Numerical Analysis of Spectral Methods: Theory and Applications, SIAM-CBMS, Philadelphia, 1977.
[3] N.K Yamaleev, M.H. Carpenter, On accuracy of adaptive grid methods for captured shocks, J. Comput. Phys. 181 (2002) 280–316.
[4] S.P. D'yakov, On the stability of shock waves, ZETF 27 (1954) 288–295.
[5] V.M. Kontorovich, Concerning the stability of shock waves, Sov. Phys. JETP 6 (1957) 1179–1180.
[6] J.W. Bates, D.C. Montgomery, The D'yakov instability of shock waves in real gases, Phys. Rev. Lett. 84 (6) (2000) 1180–1183.
[7] K.M. Peery, S.T. Imlay, Blunt body flow simulations, AIAA Paper 88-2924, 1988.
[8] J.-Ch. Robinet, J. Gressier, G. Casalis, J.-M. Moschetta, Shock wave instability and the carbuncle phenomenon: same intrinsic origin?, J. Fluid Mech. 417 (2000) 237–263.
[9] J.J. Quirk, A contribution to the great Riemann solver debate, Int. J. Numer. Meth. Fluids 18 (1994) 555.
[10] J. Gressier, J.-M. Moschetta, Robustness versus accuracy in shock-wave computations, Int. J. Numer. Meth. Fluids 33 (2000) 313–332.
[11] J.-F. Coulombel, S. Benzoni-Gavage, D. Serre, Note on a Paper by Robinet, Gressier, Casalis and Moschetta, J. Fluid Mech. 469 (2002) 401–405.
[12] V.V. Rusanov, A blunt body in a supersonic stream, Annu. Rev. Fluid Mech. 8 (1976) 377–404.
[13] W.D. Hayes, R.F. Probstein, Hypersonic flow theory, Inviscid Flows, vol. 1, Academic Press, New York, 1966.
[14] C.C. Lin, S.I. Rubinov, On the flow behind curved shocks, J. Math. Phys. 27 (1948) 105–129.
[15] P.R. Garabedian, H.M. Lieberstein, On the numerical calculation of detached bow shock waves in hypersonic flow, J. Aero Sci. 25 (1) (1958) 109–118.
[16] M.D. Van Dyke, The supersonic blunt-body problem – review and extension, J. Aero/Space Sci. 25 (4) (1958) 485–496.
[17] M.W. Evans, F.H. Harlow, Calculation of supersonic flow past an axially symmetric cylinder, J. Aero Sci. 25 (1) (1958) 269.
[18] G. Moretti, M. Abbett, A time-dependent computational method for blunt body flows, AIAA J. 4 (12) (1966) 2136–2141.
[19] M.Y. Hussaini, D.A. Kopriva, M.D. Salas, T.A. Zang, Spectral methods for the Euler equations: Part 2. Chebyshev methods and shock-fitting, AIAA J. 23 (2) (1985) 234–240.
[20] D.A. Kopriva, T.A. Zang, M.Y. Hussaini, Spectral methods for the Euler equations: the blunt body problem revisited, AIAA J. 29 (9) (1991) 1458–1462.
[21] D.A. Kopriva, Shock-fitted multidomain solution of supersonic flows, Comput. Meth. Appl. Mech. Eng. 175 (1999) 383–394.
[22] G.P. Brooks, J.M. Powers, A Karhunen–Loève Galerkin technique with shock-fitting for optimization of a blunt body geometry, AIAA Paper 2002-3861, 2002.
[23] C. Canuto, M.Y. Hussaini, A. Quarteroni, T.A. Zang, Spectral Methods in Fluid Dynamics, Springer, New York, 1988.
[24] D. Gottlieb, J.S. Hesthaven, Spectral methods for hyperbolic problems, J. Comput. Appl. Math. 128 (2001) 83–131.
[25] B. Fornberg, A Practical Guide to Psuedospectral Methods, Cambridge University Press, Cambridge, 1998.

[26] B.A. Finlayson, The Method of Weighted Residuals and Variational Principles, Academic Press, New York, 1972.
[27] K.W. Thompson, Time dependent boundary conditions for hyperbolic systems, J. Comput. Phys. 68 (1987) 1–24.
[28] K.W. Thompson, Time dependent boundary conditions for hyperbolic systems, II, J. Comput. Phys. 89 (1990) 439–461.
[29] G.P. Brooks, A Karhunen–Loève least-squares technique for Optimization of Geometry of a Blunt Body in Supersonic Flow, Ph.D. Dissertation, University of Notre Dame, Notre Dame, IN, 2003.
[30] A.C. Hindmarsh, ODEpack, A systematized collection of ODE solvers, in: R.S. Stepleman et al. (Eds.), Scientific Computing, North-Holland, Amsterdam, 1983, p. 55.
[31] L.R. Petzold, Automatic selection of methods for solving stiff and nonstiff systems of ordinary differential equations, SIAM J. Sci. Comput. 4 (1983) 136.
[32] G.I. Taylor, J.W. Maccoll, The air pressure on a cone moving at high speeds, Proc. R. Soc. A 139 (1933) 278–311.
[33] L. Lees, Hypersonic flow, in: Proceedings of the Fifth International Aeronautical Conference, Los Angeles, Institute of the Aeronautical Sciences, New York, 1955, pp. 241–276.
[34] J.D. Anderson, Hypersonic and High Temperature Gas Dynamics, McGraw-Hill, New York, 1989.
[35] F.S. Billig, Shock-wave shapes around spherical and cylinder-nosed bodies, J. Spacecraft Rockets 4 (6) (1967) 822–823.